Final Report

May 1977
NASA CR-145179

DESIGN OF AN AIRBORNE LIDAR FOR STRATOSPHERIC AEROSOL MEASUREMENTS

By: W. E. EVANS

Prepared for:

NATIONAL AERONAUTICS AND SPACE ADMINISTRATION
LANGLEY RESEARCH CENTER
HAMPTON, VIRGINIA 23365

NASA
National Aeronautics and
Space Administration

CONTRACT NAS1-14520

SRI Project 5557

Final Report

May 1977
NASA CR-145179

DESIGN OF AN AIRBORNE LIDAR FOR STRATOSPHERIC AEROSOL MEASUREMENTS

By: W. E. EVANS

Prepared for:

NATIONAL AERONAUTICS AND SPACE ADMINISTRATION
LANGLEY RESEARCH CENTER
HAMPTON, VIRGINIA 23365

NASA
National Aeronautics and
Space Administration

CONTRACT NAS1-14520

SRI Project 5557

Approved by:

RONALD T. H. COLLIS, *Director*
Atmospheric Sciences Laboratory

RAY L. LEADABRAND, *Executive Director*
Electronics and Radio Sciences Division

Copy No. ____

Page
Intentionally
Left Blank

CONTENTS

Page
Intentionally
Left Blank

ABSTRACT

This study concentrates on the engineering aspects of implementing a stratosphere-monitoring lidar that could be used aboard the NASA CV990 or some similar large jet aircraft capable of operating anywhere in the world. The principal objective was to define a system that would be appropriate for providing validation data for the SAM-II and SAGE limb-scanning solar photometers to be flown aboard the Nimbus G and AEM-B satellites currently scheduled for launching in late 1978 and mid-1979, respectively.

A system analysis section provides background data on expected signal and noise levels, a variety of hardware options are proposed spanning a range from use of the existing SRI Mark IX ruby lidar plus an expanded digital data recording system to the development of completely new lidar employing a high prf Nd:YAG laser.

To gain a relatively large receiver collection aperture without requiring extensive modifications to the aircraft, a modular, multiple-telescope receiving concept is developed. This concept, together with the choice of a specific photodetector, signal processsing, and data recording system capable of maintaining approximately 1% precision over the required large signal amplitude range, is found to be common to all of the options.

It is recommended that development of the lidar begin by more detailed definition of solutions to these important common signal detection and recording problems.

Page
Intentionally
Left Blank

ILLUSTRATIONS

TABLES

I INTRODUCTION, BACKGROUND, AND OBJECTIVE

Ground-based and airborne lidar systems have been used effectively to determine the vertical distribution of aerosol particulate backscattering in the stratospheric region. By applying appropriate optical scattering models, backscatter data can be interpreted in terms of aerosol optical parameters (such as extinction) and physical parameters (such as mass concentration) required for evaluating the likely climatic impact of natural and anthropogenic stratospheric modification.

For upper atmosphere investigations, an airborne lidar system possesses two distinct advantages over ground-based equivalents. First, it can provide data in global regions where surface-based measurements are difficult to make, as for example over the oceans or in winter polar regions. Second, for a given lidar configuration, system accuracy and precision are improved both by locating the lidar closer to the targets being measured and through elimination of the highly variable path attenuation of clouds and other tropospheric aerosols.

The principal impetus for this particular study is the anticipated need to obtain corroborative data on the vertical distribution of upper atmosphere aerosols where and when measurements are to be made by the SAM-II and SAGE limb-scanning photometer instruments on the Nimbus G and AEM-B satellites, currently scheduled for launching in late 1978 and mid-1979, respectively.

The detailed objectives as spelled out in the contract work statement and addressed in this report can be interpreted generally as the consideration of available options for fielding the desired data validation experiments both before and after the satellite launch. The principal instrument platform considered is the NASA Convair 990 flying laboratory based at Ames Research Center, Moffett Field, California. The information desired was:

- The performance to be expected if the existing SRI general-purpose atmospheric ruby (Mark IX lidar were flown.

- Modifications that might be made to the Mark IX lidar to facilitate obtaining more useful data at minimum expense.

- Definition of a new lidar design, specifically directed toward the needs as now defined.

- Time and cost factors for the various options.

The precision, spatial resolution, and temporal resolution that should be sought in order to provide a valid check on the results of the SAM-II experiment currently are being studied by members of the SAM-II Nimbus Experiment Team (NET). Their findings, together with the information in this report on capabilities and limitations of available hardware, should permit valid decisions to be made about how to proceed before and during the actual data validation phase.

II METHOD OF APPROACH

In Section III (System Calculations) the expected performance of the existing SRI Mark IX lidar is examined assuming airborne operation against typical stratospheric aerosol targets. The results of this examination disclosed early in the investigation that while the existing equipment configuration might be useful in providing baseline checks relatively quickly, there was a strong probability that the performance at either wavelength would be considered marginal for use during the SAM II mission. That is, even if a pulse-counting capability were added it would require barely tolerable amounts of integration time to produce results competitive with those expected from SAM II.

It was also apparent that significant improvements in overall system performance could be expected through changes in the receiving system alone and that these changes could be implemented relatively easily at moderate cost.

One such change would involve the subsitution of a newer, higher quantum efficiency photomultiplier that would increase the number of photoelectron counts per photon by a factor of approximately six. Another change would be to employ a larger receiver collection aperture. For operation at relatively short ranges in the lower troposphere the existing 6" diameter receiving telescope is quite adequate and helps provide a compact lidar. On the other hand, for long range, upper atmosphere studies it is axiomatic that one strives for as much receiver light-collecting area as possible. The first step in this direction would be to attempt to utilize most if not all of the clear aperture of one of the upward-looking windows of the CV 990 aircraft for receiving. By transmitting through a separate, adjacent window, one could minimize problems of receiver paralysis and of background due to residual pump light and/or laser rod fluorescence, by backscattering from the window. An effective

area increase by a factor of 4.6 could be obtained by converting to a single 14-inch receiving telescope. Still more collecting area could be realized by using more than one window for receiving. This line of reasoning led to the concept of a modular receiver, employing an optional number of relatively low-cost receiving telescopes, all converged on the same transmitter beam and having their optical outputs channeled to a single high quality photodetector.

This modular receiver design concept has been considered in some detail during this study and appears to be well suited to the needs of an airborne stratospheric lidar. It provides a desirable flexibility to adapt to currently unknown amounts of space that may be available on the CV 990, to possible use on other aircraft, and to available hardware budgets. Thus the material that follows addresses not only (1) the provision of an existing lidar, and (2) a completely new lidar system, as specified in the contract work statement, but also something of a continuum of options between these two extremes.

To provide some perspective on the relative amount of space devoted in this report to the multiple receiver concept, it must be admitted that the author's early goals for aperture-derived measurement precision were greater than could be defended for the SAM II and SAGE application later in the study after more thought and discussions with Dr. P.B. Russell about other error sources (see Section III-C). However, descriptions of the multiple receiver design options have been retained in the event that they might prove useful, perhaps, for another application.

As previously mentioned, attention has been confined to two wavelength regions. The ruby wavelength remains a strong contender not only because it is one that can be implemented most quickly and at least cost using existing field-proven hardware, but also because of a strong conviction that for atmospheric probing it provides a near-optimum compromise among a number of conflicting system constraints. The basis for this conviction is set forth in the sections to follow.

In Section III-C it is shown that for equivalent transmitted energy, one must integrate approximately three times as long at 1.06 μm to achieve the same measurement precision as can be obtained at 0.694 μm. To attain even this level of comparison, one must exploit the very significant recent advances in 1.06 μm detector performance (that is, a factor of 40 increase in quantum efficiency (q.e.) combined with much lower internal noise). In Section VIII it is pointed out that these improvements command a very real premium both in dollars and in operating at 1.06 μm is the desire to make measurements at the same wavelength employed by the SAM-II instrument, thereby eliminating some of the uncertainties involved in comparing back-scattering at one wavelength to extinction at another. It is also important to note that for a given aerosol particle concentration, the ratio of particulate to molecular backscattering at 1.06 μm is appreciably larger than at 0.69 μm. Hence, a larger uncertainty in measurement of the lidar signal can be tolerated and still lead to smaller relative errors in the infrared particulate component of backscattering or extinction. Another factor in favor of Neodymium is the ability to frequency double to achieve 0.530 μm (green), a wavelength that is possibly of use for particle size distribution experiments.

For these reasons, we consider in Sections IV-B and V what would be required to convert the Mark IX lidar to operate at 1.06 μm.

For a brand new lidar dedicated to airborne stratospheric aerosol probing, the weight of evidence appears to be more completely on the side of neodymium largely because of the greater amount of military-sponsored engineering effort that has gone towards reducing size, weight, and power consumption of reliable Nd:YAG laser systems. An airborne lidar system design incorporating a state-of-the-art, high repetition rate Nd:YAG laser operating in conjunction with one or more of the modular 14-inch receiver units is described in Section IX.

"Page missing from available version"

p. 6.

III SYSTEM CALCULATIONS

A. General

In order to simplify the task of evaluating how various proposed changes in system parameters affect the accuracy of the final output data products, we will maintain separate accounts of four major components of the lidar output signal. These four components will be called N_R, N_P, N_B, and N_I, and are defined as the photoelectron count rate for any given range interval that results from Rayleigh molecular backscattering (N_R), from Mie or particulate backscattering (N_P) from sky background light (N_S), and from spurious internal system noise (N_I).

N_R and N_M can be calculated from the lidar equation:

$$N_R = \frac{U_T A_R T_o}{2h R^2} T_a^2 \lambda \beta_R q \qquad (1)$$

$$N_P = \frac{U_T A_R T_0}{2h R^2} T_a^2 \lambda \beta_P q \qquad (2)$$

where:

U_T = transmitter energy per pulse actually radiated (Joules) (The transmitted pulse length is assumed to be much less than the range integration period)

A_R = receiver effective aperture area (m^2) (Includes effect of all mechanical aperture blockages but not of optical transmission factors.)

T_O = overall optical transmission factor for all receiver components in tandem

T_a^2 = two-way atmospheric transmission factor to range R and for wavelength λ

λ = operating wavelength (meters)

β_R, β_P = volume backscattering coefficients (at wavelength λ) for molecular Rayleigh and particulate scatters, respectively. (meters^{-1} - steradian^{-1})

q = detector quantum efficiency at wavelength λ

h = Planck's constant; 6.625×10^{-34} Joule - second.

R = slant range to the point of measurement (meters)

Background Noise

N_B = is a function of the receiver only and can be either measured empirically or calculated from Equation (4) of Section III-B4.

N_I is determined by the type and temperature of the detector. It must be estimated from manufacturer's specification and/or measured for the specific components used.

Although we find it convenient to speak of pulse "counts" while tracing the effects of various system design alternatives on the statistics of the detection and measurement process, we should point out here that for stratospheric aerosol monitoring the photoelectron pulse rate often will be too high to separate and count reliably in an actual digital counter. Instead, a measure of the photoelectron count (photon absorption rate) will be obtained by integrating the (amplified) current pulses in a storage capacitor and measuring the accumulated voltage at the end of each range interval with a fast analog-to-digital converter, that is, a Biomation Model 8100 transient recorder. The "counting" type of signal-to-noise (S/N) analysis will still apply as long as the total number of photoelectrons per range interval is large enough to effectively smooth the spurious pulse-to-pulse variations in photomultiplier current gain. In order to make this assumption as nearly valid as possible, we propose the use of a photomultiplier specifically designed to minimize the spread of the single electron pulse height distribution. The Varian VPM164M (visible) or VPM164A (infrared) appear to be such devices, when fitted with the Gallium Phosphide first dynode option.

B. Performance at 0.6943 μm and 1.06 μm

In this section we calculate performance at both $\lambda = 0.6943$ μm and $\lambda = 1.06$ μm for several systems designed around nominal 1 Joule per pulse, 1 pulse per second transmitters. The results provide a set of data that not only is easily scaled for other transmitter characteristics but also is directly applicable to the SRI Mark IX lidar transmitter, either in its existing ruby configuration or after conversion to use a Nd:YAG laser rod. Since the ruby lidar could be fielded most quickly and at least expense it will be considered the baseline system. Parameters differing at the neodymium wavelength will be listed as required.

1. Equipment Parameters

Table I lists numerical values for the pertinent lidar system parameters.

2. Atmospheric Parameters

Values for the volume backscatter coefficient β_{180} due to the molecular atmosphere at various altitudes are listed in Table II and plotted in Figure 1. The second column of Table II lists the atmospheric molecular number densities that form the bases for calculating backscattering. The backscattering coefficients listed for each wavelength were obtained by multiplying the number densities in Column 1 by the Rayleigh single particle backscattering cross section, C_R, appropriate to that wavelength as given at the bottom of the table.

Table III lists approximate values for volume backscatter coefficients, $\beta_p(\lambda)$ due to the particulate content at various elevations for "moderate post volcanic" conditions. The values are derived from the Rayleigh backscattering coefficients of Table II and the time-averaged scattering ratios measured by Russell et al (1976) at $\lambda = 0.694\mu m$ during the 1975 recovery from the Fuego volcanic injection. Backscattering coefficients for the neodymium wavelength were derived from the ruby wavelength values by

Table I

SYSTEM PARAMETERS FOR SRI MARK IX LIDAR AND VARIATIONS

Symbol	Definition	Units	System					
			Unmodified	1 Aux RCVR		2 Aux RCVRS		4 Aux RCVRS	
U_T	Radiated transmitter, energy per pulse (pulse length << integration period)	J	1	1		1		1	
A_R	Receiver effective aperture area. Includes effect of mechanical aperture blockage but not of optical transmission factors	m^2	0.0174	0.080		0.160		0.320	
T_O	Receiver optical transmission factor. All components in tandem	- - - -	0.25	0.25		0.25		0.25	
λ	Wavelength	m	0.694E- 6	0.694 E-6	1.06 E-6	0.694 E-6	1.06 E-6	0.694 E-6	1.06 E-6
q	Detector quantum efficiency at wavelength λ	- - - -	0.025	0.15	0.02	0.15	0.02	0.15	0.02
W_R	Receiver angular field of view	sr	$\frac{\pi}{4}$(0.49)E-6	$\frac{\pi}{4}$(0.49)E-6		$\frac{\pi}{4}$(0.49)E-6		$\frac{\pi}{4}$(0.49)E-6	
$\Delta\lambda$	Optical filter bandwidth	Å	10	10		10		10	

Table II

MOLECULAR NUMBER DENSITIES
AND RAYLEIGH VOLUME BACKSCATTER
COEFFICIENTS AT VARIOUS ALTITUDES

Elevation km	N, m^{-3} (a)	β_R(0.53 μm), m^{-1} sr^{-1}	β_R(0.694 μm), m^{-1} sr^{-1}	β_R(1.06 μm), m^{-1} sr^{-1}
0	2.55E25	1.588E-6	5.391E-7	9.922E-8
10	8.599E24	5.354E-7	1.818E-7	3.330E-8
20	1.849E24	1.152E-7	4.004E-8	7.370E-9
30	3.714E23	2.312E-8	7.851E-9	1.445E-9
40	8.324E22	5.183E-9	1.760E-9	3.239E-10
50	2.252E22	1.402E-9	4.761E-10	8.763E-11
60	7.262E21	4.521E-10	1.535E-10	2.826E-11
70	2.088E21	1.300E-10	4.414E-11	8.124E-12
80	4.503E20	2.804E-11	9.519E-12	1.752E-12
90	8.309E19	5.173E-12	1.757E-12	3.233E-13
100	1.62E19	1.009E-12	3.425E-13	6.303E-14

$\beta_R(\lambda) = N\ C_R\ (\lambda)$, where

C_R (0.694 μm) = 2.114E-32 m^2 sr^{-1} [b]
C_R (1.06 μm) = 3.891E-33 m^2 sr^{-1} [c]
C_R (0.530 μm) = 6.226E-32 m^2 sr^{-1} [c]

---

[a] Source: U.S. Air Force Handbook of Geophysics for Air Force Designers, ARCRC, 1957.

[b] Source: Russell, P. B.; Viezee, W.; and Hake, R. D.: 1976[a].

[c] C_R (0.694 μm) $\times \left(\frac{\lambda 2}{\lambda 1}\right)^{-4}$.

Table III

PARTICULATE VOLUME BACKSCATTERING COEFFICIENTS

	Scattering Ratio $\frac{\beta_P + \beta_R}{\beta_R}$ Moderate Volcanic		Volume Backscatter Coefficient, m^{-1} sr^{-1}			
h km	1.06 μm (b)	0.694 μm (a)	β_R(1.06 μm) (c)	β_R(0.694 μm)	β_P(1.06 μm)	β_P(0.694 μm)
5	1.40	- - - -	- - - -	- - - -	- - - -	- - - -
10	1.40	1.11	3.330E-8	1.82E-7	1.33E-8	2.00E-8
15	2.50	1.34	- - - -	- - - -	- - - -	- - - -
20	2.80	1.51	7.370E-9	4.00E-8	1.33E-8	2.04E-8
25	1.40	1.31	- - - -	- - - -	- - - -	- - - -
30	1.25	1.07	1.445E-9	7.85E-9	3.61E-10	5.50E-10
35	1.15	- - - -	- - - -	- - - -	- - - -	- - - -
40	1.08	1.01	3.239E-10	1.76E-9	2.59E-11	- - - -

[a] Source: 1975 average results of Russell, Viezee, and Hake, 1976[b].

[b] Source: Derived from (a), assuming $\beta_P \propto \lambda^{-1}$.

[c] Source: Table II.

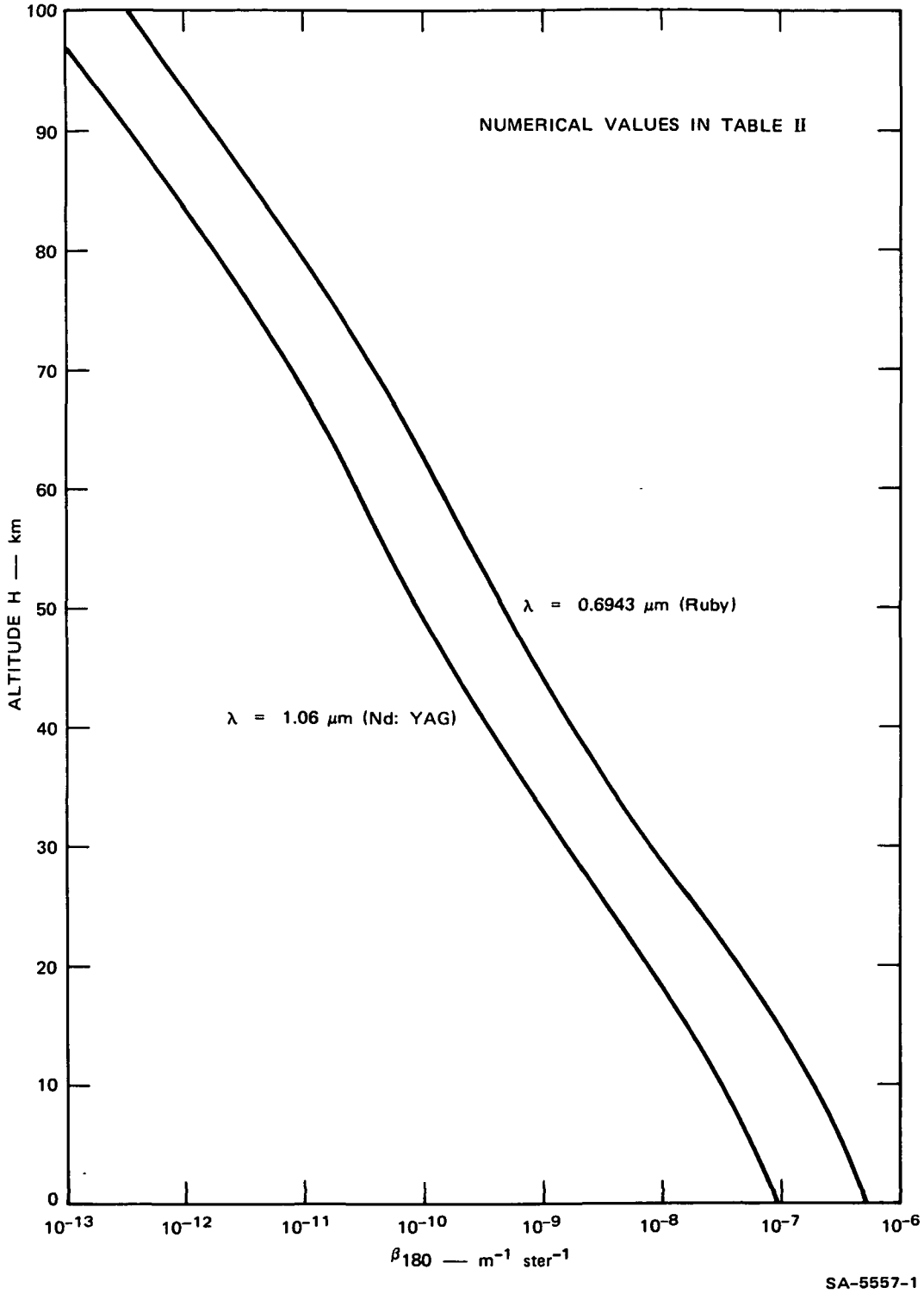

FIGURE 1 VOLUME BACKSCATTER COEFFICIENTS VERSUS ALTITUDE FOR THE MOLECULAR ATMOSPHERE

assuming a λ^{-1} wavelength dependence; that is,

$$\frac{\beta_{1060\ nm}}{\beta_{694\ nm}} = \frac{\lambda 1}{\lambda 2} = \left(\frac{1060}{694}\right)^{-1} = 0.655 \qquad (3)$$

This wavelength dependence is consistent with the optical models of the stratospheric aerosol derived from measurement data by Pinnick et al. (1976).

3. Expected Lidar Signal Returns

Solutions of the lidar equation at both ruby and neodymium wavelength are plotted in Figures 2,3, and 4 for the lidar parameters, Rayleigh, and particulate backscatter coefficients just discussed. For all cases, it was assumed that the lidar was flying at an altitude of 10 km (33,000 ft).

Additionally, these curves assume perfect receiver/transmitter convergence at all ranges and thus represent the maximum available signal. Finite transmitter-receiver separations will modulate these maximum predicted signals downward at some altitudes as discussed in Section V.

4. Sky Background Signal

The receiver photoelectron count due to background light N_B, is given by:

$$N_B = B_B A_R T_O \omega_R \Delta\lambda \frac{\lambda}{hc} q \qquad (4)$$

Where:

B_B = background sky radiance in the direction of view (watts - meter^{-2} - steradian^{-1} - Angstrom^{-1}

ω_R = receiver solid angular field of view (steradians)

$= \frac{\pi}{4} \theta_R^2$

θ_R = receiver full beamwidth (radians)

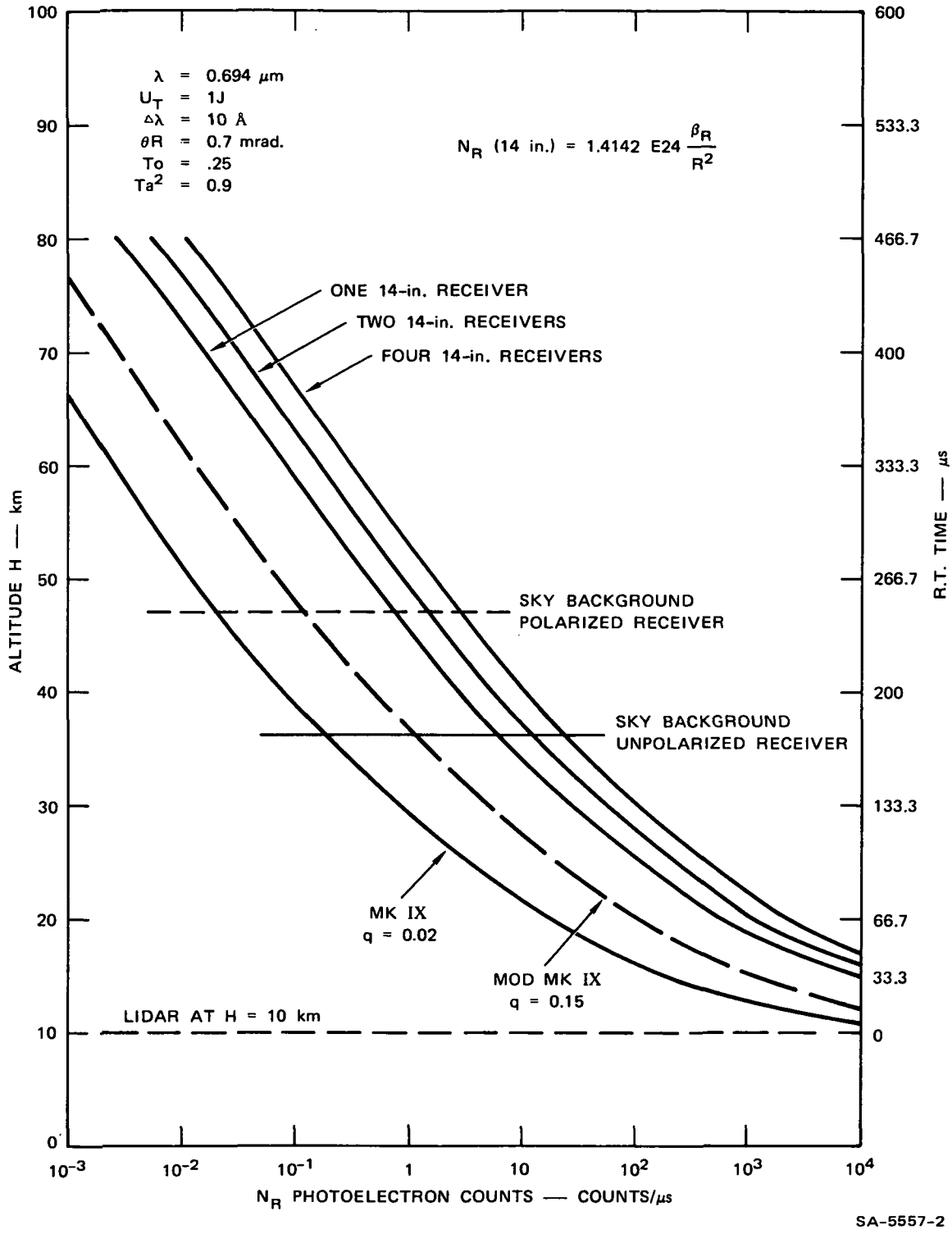

FIGURE 2 SIGNAL RETURN RESULTING FROM RAYLEIGH MOLECULAR BACKSCATTERING — RUBY SYSTEM

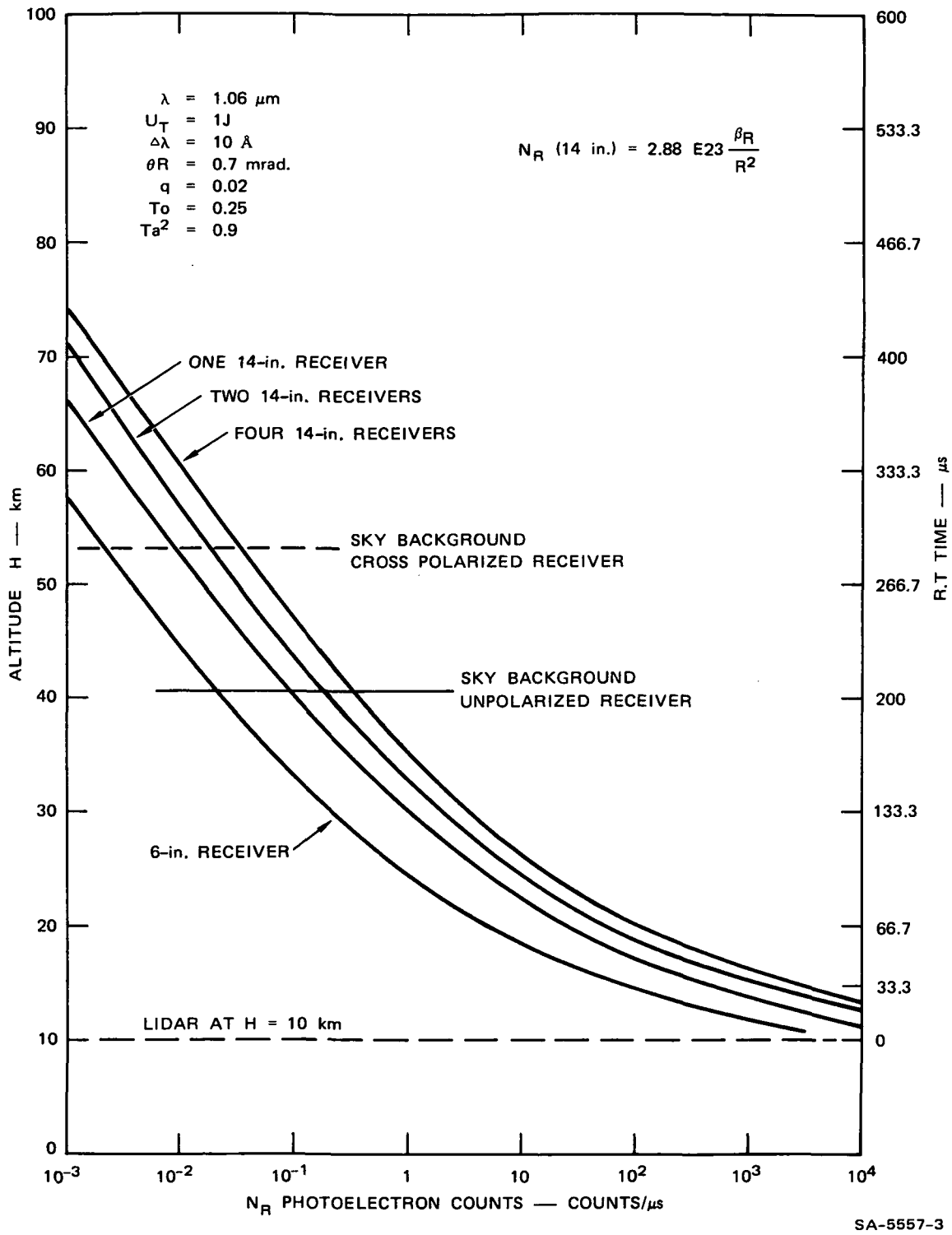

FIGURE 3 SIGNAL RETURN RESULTING FROM RAYLEIGH MOLECULAR BACKSCATTER — Nd SYSTEM

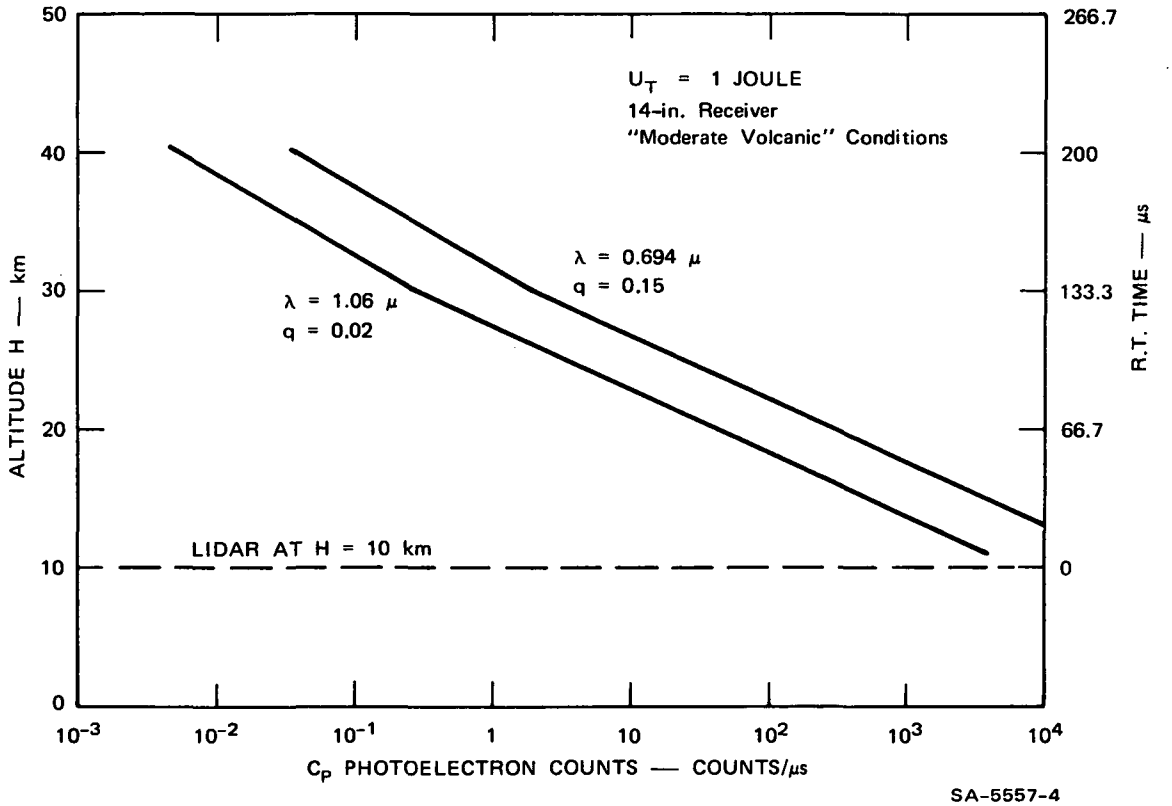

FIGURE 4 SIGNAL RETURN RESULTING FROM PARTICULATES

$\Delta\lambda$ = receiver narrow band filter bandwidth ($\mathring{A}$ngstroms)
full width, half amplitude

c = velocity of light = 3×10^8 m - sec^{-1}

and the other parameters are as previously defined.

A plethora of often-conflicting data is available on sky background radiances, tabulated in a variety of units, relative and absolute. For the particular geometry involved in validation flights for the SAM-II experiment; that is, for zenith viewing and low sun elevation, the agreement among various sources is fair and the values given and referenced in Figure 5 have been selected for engineering systems evaluation.

The skylight will be strongly polarized, and for at least some portions of the experiment this fact might be exploited to reduce the background noise count by perhaps an order of magnitude. Figure 6 shows the path geometry, approximately to scale. For the proposed high noon, sun-synchronous orbit, the zenith skylight viewed from the aircraft will have its electric vector polarized perpendicular to the plane of the orbit (and the plane of the paper). For a flight plan designed to sample along the satellite-to-sun path near the tangent point, the aircraft would be flying either directly into or directly away from the sun, and the sky background interference could be minimized by orienting the lidar so that both transmitter and receiver were polarized parallel to the flight line. Provision for this adjustment has been made in the transmitter and receiver mounting designs proposed herein.

Background sky count computed from equation (4) for the receiver parameters of Table I, and sky radiances a factor of ten less than those given in Figure 5 (to account for polarization), are shown as dashed lines on the signal return plots, Figures 2 and 3.

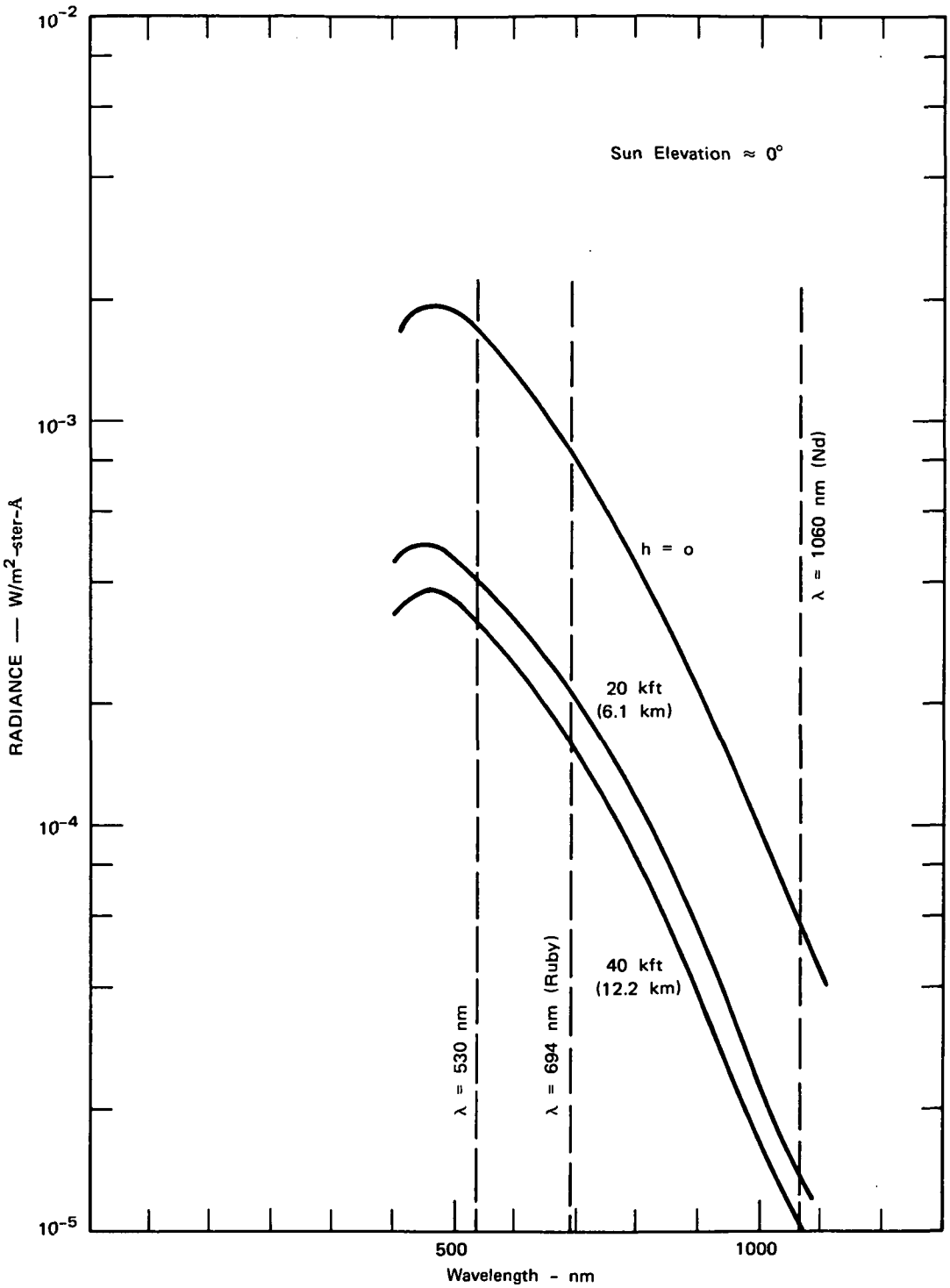

SOURCES: Quasius & McCanless (1966), Handbook of Geophysics (1960), and Duntley (1958)

SA-5557-5

FIGURE 5 ZENITH SKY RADIANCE

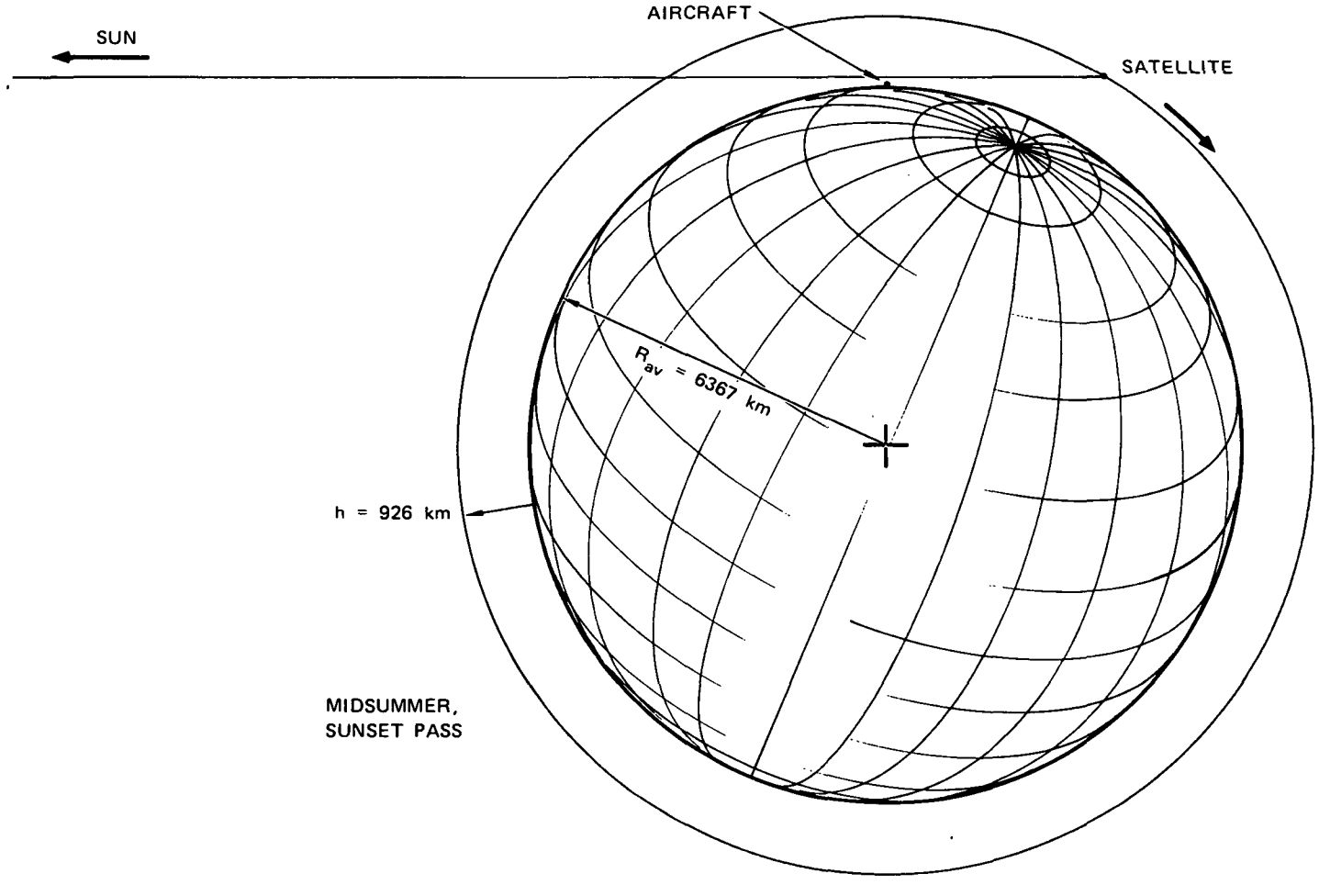

NOTE: Zenith Sky above aircraft is strongly polarized with electric vector perpendicular to plane of the paper.

SA-5557-6

FIGURE 6 VIEWING GEOMETRY FOR SAM II DATA VALIDATION LIDAR FLIGHTS

Note that with all other factors unchanged, the background noise count will match the lidar signal return from some particular elevation, independent of the size of the receiver aperture.

Nighttime sky radiances are more difficult to predict because of the effect of the moon and other factors. First order estimates can be based on the following:

- With a full moon near the horizon, zenith sky radiances should be less than the solar induced radiances of Figure 5 by about a factor of 10^6 (the ratio of sun and moon radiances).

- For a full moon close to the zenith (never attainable in high latitudes), the nighttime sky radiance might be only 10^4 less than values given in Figure 5.

- Minimum values of zenith sky radiance obtainable on moonless nights will approximate the airglow which according to Allen (1955) is 7×10^{-10} watts/m^2 - ster - Å at $\lambda = .7$ micrometers, a value actually slightly greater than one might expect at high altitudes with a full moon near the horizon (per the first consideration above). Other references, for example Quasius and McCanless (1966), quote average values of 5×10^{-11} watts/m^2 - ster - Å for the night sky in the visible region.

5. Internal Detector Noise

The dark noise count versus temperature for the recommended photomultiplier tubes, Varian VPM 164M and VPM 164A (formerly VPM 163 and VPM 164), is given in Figure 7. By comparison with the background noise count shown on Figures 2 and 3 it can be seen that little or no cooling is required to keep the Galium Arsenide (ruby wavelength) tube noise count negligibly small (< 1%) with respect to the expected sky background.

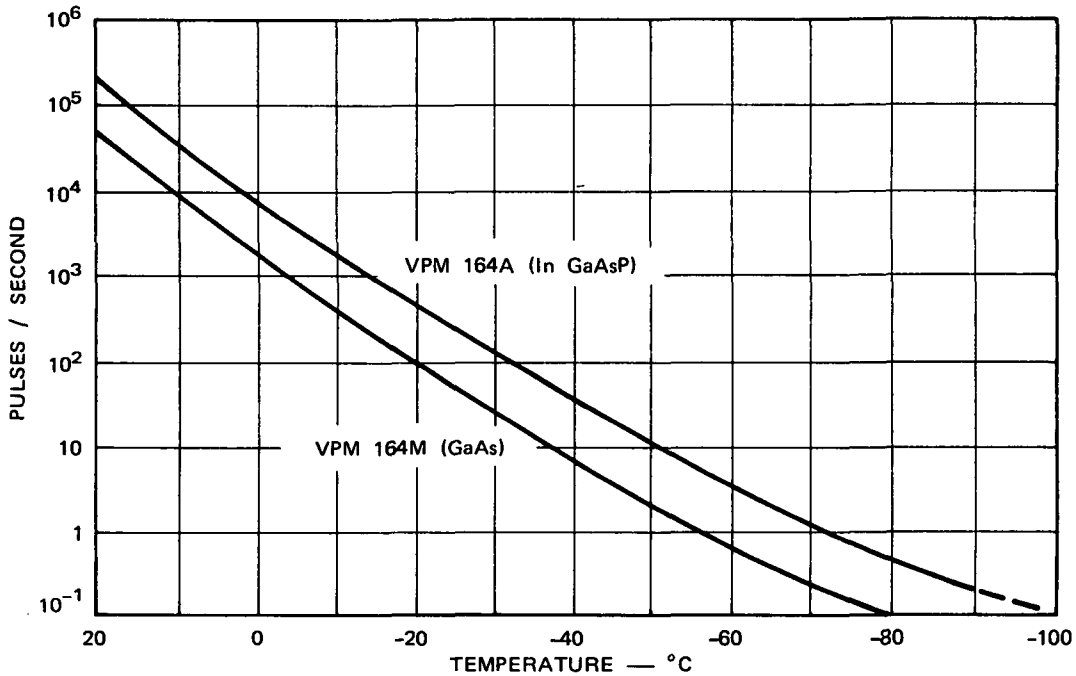

SOURCE: Adapted from manufacturer's data sheet.

SA-5557-7

FIGURE 7 DARK NOISE COUNT VERSUS TEMPERATURE FOR VARIAN PHOTOMULTIPLIERS

On the other hand, a temperature of -20°C, which is the lowest that can be conveniently attained with a thermoelectric cooler, would be barely adequate to bring the noise count for an Indium Galium Arsenide Phosphide (Neodymium band) tube down to less than 10% of the expected background noise count from a polarized 14" receiver.

C. Discussion and Test Cases

Two principal figures of merit were used in this study to compare the performance to be expected from various system alternatives. These criteria are the particulate and total signal-to-noise ratios, given respectively by

$$S_P/N = \frac{N_P}{\sqrt{N_P + N_R + N_B + N_I}} \tag{5a}$$

and

$$S_T/N = \frac{N_R + N_P}{\sqrt{N_P + N_R + N_B + N_I}} \tag{5b}$$

where N_P, N_R, N_B, and N_I are the photoelectron pulse counts at the output of the photodetector, accumulated for a particular range bin, as a result of backscattering from aerosol particles, from the Rayleigh molecular environment, from continuous radiation (background light), and from internal detector noise.

S_P/N (Equation 5a) expresses the ratio of the inferred particle-responsive component, N_p, to the uncertainty in measuring the total lidar return from a given altitude; its inverse is the lidar-dependent component of the relative uncertainty in lidar-measured particulate backscattering at that altitude; that is, it is basically a measure of instrumental precision.

While a number of calculations of S_P/N were made during the early part of this study and are included in this report for reference and completeness, later discussions with P.B. Russell revealed that because of the way that upper atmosphere lidars are normally operated S_P/N can be both misleading and over-ambitious as a system figure of merit except, perhaps, for the relatively infrequent situations where particulate backscattering exceeds molecular backscattering (scattering ratio R greater than two). For more usual stratospheric conditions the uncertainty components arising from sources independent of the lidar equipment parameters will predominate and provide a practical limit on the instrumental precision worth seeking.

This result comes about because the factor relating S_P and the desired result, the particulate backscatter coefficient, is not a fixed system constant (even for a given range) but is, in effect, derived for each lidar shot or group of shots through a normalizing process that assumes molecular backscattering from clean air (negligible contribution from particulate backscattering) at some calibration range point on the profile. Any errors in the validity of this "clean air" assumption, or any errors in the knowledge of either the density profile or the optical transmission between the normalization range and the measurement range will then contribute errors to results deduced from the measurement. The magnitude of these contributing errors or uncertainty factors has been investigated by Russell et al. (1976a). They found typical relative uncertainties of 1% each for the density and transmission factors and 0.1 $(R_{max}-1)$ for the normalizing error, where R_{max} is the maximum scattering ratio encountered. In practice, it is the scattering ratio,

$$R = \frac{\beta_P + \beta_M}{\beta_M}$$

that is most often computed and reported by stratospheric aerosol investigators.

The above-discussed uncertainties were shown to affect the scattering ratio as follows:

$$\text{relative error in scat. ratio, } R \equiv \frac{\sigma(R)}{R} = \qquad (6)$$

$$\sqrt{\left(\begin{array}{c}\text{relative error}\\ \text{in clean air}\\ \text{assumption}\\ 0.1(R_{max}-1)\end{array}\right)^2 + \left(\begin{array}{c}\text{relative error}\\ \text{in air density}\\ \text{specification}\\ \approx 0.01\end{array}\right)^2 + \left(\begin{array}{c}\text{relative error}\\ \text{in two-way}\\ \text{optical trans-}\\ \text{mission}\\ \approx 0.01\end{array}\right)^2 + \left(\begin{array}{c}\text{relative error}\\ \text{introduced}\\ \text{by lidar}\\ N/S_T\end{array}\right)^2}$$

The relative uncertainty of the particulate volume backscatter coefficient derived from the lidar data was shown to be:

$$\frac{\sigma(\beta_P)}{\beta_P} = \sqrt{\left(\frac{\sigma(\beta_R)}{\beta_R}\right)^2 + \left(\frac{\sigma(R)}{R-1}\right)^2} \approx \frac{\sigma(R)}{R}\ \frac{R}{R-1} \qquad (7)$$

Study of equations (6) and (7) gives an insight into the lack of sensitivity of one desired end product, the particulate backscatter coefficient, to very high lidar measurement precision as measured by N/S_P.

Particularly at high altitudes it appears more informative to use S_T/N (equation 5b) as a figure of merit for the lidar instrument. As shown by equation (6), the inverse of S_T/N gives the lidar's contribution to the relative uncertainty in measured scattering ratio, R. This relative uncertainty in R is also the absolute uncertainty in lidar-measured β_p, expressed as a fraction of the total backscattering coefficient, $\beta_T = \beta_P + \beta_R$. The examples given below will show the usefulness of S_T/N as a figure of merit for those altitudes and wavelengths where β_P is only a few percent or less of β_R.

In Appendix A, numerical values for both S_P/N and S_T/N have been calculated for a number of test cases. The arithmetic is reproduced in sufficient detail to clearly display the relative importance of the four main noise sources for each case. Input data were taken from the graphs and tables of the preceeding section, where all count rates are expressed in units of pulses per microsecond. For the test cases, the usual pattern was to first compute S/N for a single lidar shot, using a range integration interval that appeared consistent with our understanding of the objectives of the SAM-II data validation program, and with the proposed data recording hardware. Next, a computation was made to determine how many shots need to be integrated (or how long the integration time should be) to achieve some desired measurement precision.

The effect of system trade-offs other than those considered here can readily be examined by appropriately modifying the input data and repeating the simple procedure of these examples.

The case studies can be summarized as follows:

- For measuring particulates at 20 km altitude, from an aircraft flying at 10 km altitude and using the criterion defined by equation 5a, 1% precision in β_P would require integration times of 17.9 minutes using the unmodified Mark IX ruby lidar (Case 4), 31 seconds using the transmitter and a single 14" receiver plus a high efficiency PMT (Case 1),2.1 minutes with a Nd:YAG 1.06 micron laser rod in the Mark IX transmitter plus a high efficiency 14" receiver (Case 2), and 13.6 seconds using a new transmitter utilizing a high repetition rate (30 pps) Nd:YAG laser (Case 3). Using the alternate criterion of seeking a precision of 1% of β_T in measuring β_P (equation 5b), the corresponding times are: 2.0 min (unmodified Mark IX, Case 4), 3.5 sec (modified ruby Mark IX, Case 1), 51 sec (modified Nd:YAG Mark IX, Case 2), and 5.7 sec (high PRF Nd: YAG, Case 3). The range integration interval used for all cases was 0.5 km. All of these 14" receiver times could be halved by converting to 4-telescope systems. The predominant noise contributor for the ruby systems is quantum noise (shot noise) from the Rayleigh signal component. For the Neodymium systems, quantum noise from the particulate signal component is strongest, by a small margin. For the 20 km altitudes, quite significant changes in beamwidth, bandwidth, polarization, or PMT cooling will affect the overall S/N and integration times only slightly.

- For probing at an altitude of 40 km, particulate backscattering β_P is poorly known, and sufficiently small compared to β_R that the S_P/N figure of merit is not really meaningful for evaluating lidar performance. Instead, we use S_T/N to show that measurement of β_P to a precision of 1% of β_T ($\approx\beta_R$) requires 19.8 min for the 1 pps, 14" ruby system (Case 6), and 9.34 hr for the equivalent 1 joule/sec Neodymium system (Case 7). When the goal is relaxed to attainment of a precision of 10% of ($\beta_T \approx \beta_R$) over range resolution, lengths of 5 km, 1.2 sec and 31 sec are required with the same respective systems.

IV TRANSMITTER EQUIPMENT CONSIDERATIONS

A. General

Three transmitting laser options are proposed for achieving the performance levels discussed in Section III.

(1) Use the existing Mark IX transmitter head. This unit, which will be described more completely in Section VII, utilizes a Holobeam series 300 Q switched laser fitted with a 3/8" x 3" ruby rod. It emits 1 joule per pulse, and is capable of operation at rates up to 1 pulse per second.

(2) Use the existing Mark IX transmitting head, but replace the ruby with a Neodymium:YAG laser rod as described more completely below.

(3) Construct a new transmitter capable of achieving appreciably higher average power output at 1.06 μm. The proposed unit employs a 1-50 pulse/second Sylvania Model 618DR Nd:YAG laser, is capable of 12.5 watts average output, and is described more completely in Section IX.

B. Conversion of Mark IX Laser to 1.06 Micron Wavelength

Consultation with the laser manufacturer (Holobeam) indicates that by substituting a Neodymium:YAG laser rod for the existing ruby, the Model 321 system could be converted to yield other parameters closely comparable to those of the ruby. That is, the converted laser system should meet the following specifications:

Center wavelength,	1060 nanometers
Energy per pulse,	1 joule maximum, .8 joule, typical
Maximum repetition rate,	60 pulses per minute
Linewidth,	.75 Angstrom
Beam divergence (with collimation)	< 3 milliradian, fwhp
Flashlamp pump energy	< 1250 joules/pulse

The principal component, a 3 x 3/8" Nd:YAG rod, is expensive (current cost $3560) but the alternative of Neodymium doped glass at $915 is unacceptable because of wide linewidth (80-100 Angstroms) and inability to operate at rates above about 4 pulses per minute because of thermal problems.

Additional changes that would be needed in the transmitter include the following:

	Parts Cost
Brewster stack polarizer and rail mount, (addition)	($) 580
1.06 μ high reflection mirror (substitution)	345
1.06 μ front etalon (substitution)	575
Beam expander, 4x, coated for 1.06 μ (subsitution)	585
	$ 2,085

Narrow-band "V" coatings are used on the beam expander. Broadband coatings will be used on all other optical components, including possibly, the aircraft windows. The present Pockels cell is rated for operation at either wavelength.

Approximately 1 week of down time should be anticipated to make the conversion the first time and to determine and document optimum pump levels, adjustments, and so on. After the first time, conversion from one wavelength and realignment at another normally will require that the lidar be removed from service for 1 or 2 days.

C. High PRF Nd:YAG Transmitter

Since the SAM-II limb-scanning sunphotometer to be carried by Nimbus G will operate at 1.06 μm, there would be some value in having corroborative airborne lidar measurements made at the same wavelength to eliminate any wavelength-dependent assumptions required to compare the data. The system calculations show that operation at 1.06 μm would require appreciably more average transmitter output power than would be the case with ruby. For

Nd:YAG, high average power is more easily and economically attained by operating a relatively small laser rod at a high PRF than by using the converse. While there appears to be no inherent advantage to the high PRF for high altitude probing--in fact it slightly complicates the data collection process--there is the opportunity to capitalize on the large amount of technology and hardware development effort that has been expended on high PRF systems for military illuminator and rangefinder applications. Largely as a result of these efforts, the additional average power required to roughly match the immediately obtainable "baseline" ruby performance could be obtained with commercially available Nd:YAG laser systems that are smaller, more easily maintained, and require less primarily input power than either the present Mark IX transmitter or readily available, newer replacements.

Added to the foregoing is the relative ease of doubling the generated laser frequency to obtain energy near the middle of the visible range (0.53 μm), thus providing a dual wavelength capability that is of interest as a means for infering particle size distributions.

Should a brand new laser transmitter seem desirable for the airborne lidar project, the foregoing arguments present a strong case for a high PRF Nd:YAG system even though the ruby wavelength still appears near optimum from the standpoint of detected photons per joule of transmitted energy.

A transmitter design utilizing a commercially available high PRF Nd:YAG laser is described in Section IX-A.

"Page missing from available version"

page 30

V RECEIVER EQUIPMENT CONSIDERATIONS

A. Existing Equipment

The present Mark IX ruby lidar utilizes a 6" Newtonian telescope and an RCA 7201 photomultiplier. As the system calculations show, the received signal levels using this combination are too low to be of serious interest for high altitude lidar probing. The reason for its being considered at all is that it is immediately available, is mounted close enough to the transmitter that both will fit under one of the CV 990 windows, and could provide a baseline system of known performance against which to check newer receivers. The modifications required to incorporate a cooled PMT housing would be quite substantial, and are not recommended. That is, if the considerable investment required to convert to 1.06 μm operation is contemplated, either via modification of the Mark IX laser or procurement of a new one, plus the procurement of an expensive high efficiency PMT, it would appear poor economy not to also convert to a larger receiver aperture by one of the means described later in this section.

B. High Performance Photomultiplier Tubes for Operation at 1.06 μm

Primarily as a result of work on classified military infrared systems very significant advances have been made over the last few years in the performance that can be obtained from photomultiplier detectors operating at 1.06 micrometers. The Varian VPM 164A appears to represent the current state of the art in devices available for unclassified projects. Its Indium Galium Arsenide Phosphide (InGaAsP) photocathode has a quantum efficiency of 2% at 1.06 micrometers. This is a very significant improvement over the 0.05% previously available in S1 photocathodes, and is about the same efficiency that has been employed in lidars for many years at the ruby wavelength, using the S20 cathode. In addition, the internally-generated noise level has been reduced to the point where, with moderate cooling, this noise component can be made negligible (less than 100 pulses per second), again comparable to the best performance available at ruby wavelength only a few years ago. The noise performance of the VPM 164A tube was plotted in Figure 7.

The price for these improvements is also impressive, however. Not only is the dollar cost high (currently $5-6K), but the tubes need constant pampering. They are shipped in dry ice and must be maintained below room temperature (preferably below -20°C) at all times, whether operating or not, in order not to invite deterioration and void the manufacturer's warranty. As a consequence, and as provided for in the receiver designs of Section IV, the receiver design must provide not only a refrigerated PMT housing, but also some means for assuring essentially continuous power for cooling. Thermoelectric coolers are available that operate simply from low voltage, typically 40-80 watts at 6 volts dc, and this combined with the good thermal insulation inherent in the cooled housings provides a means for transporting the tube safely from an aircraft to a motel room or laboratory between missions, but the annoyance factor would certainly be very real.

C. Proposed Use of 14-inch Celestron Telescopes

The 14-inch "Celestron" Schmidt-Cassegrain telescope with an effective focal length of 154 inches (3.91 m) is proposed as a basic receiver building block. The aperture closely matches the area of the optical windows in the NASA CV 990 aircraft, the design is compact, and lightweight yet rugged, and the instrument is produced in sufficient quantity to be moderately priced. 14" and 16" Celestron telescopes have been incorporated into two previous SRI lidar designs with entirely satisfactory results. Figure 8 is a photograph of the standard 14-inch telescope, shown on a tripod and yoke that would not be required for the lidar. Figure 9 shows the telescope mounted under one of the upward-viewing 65° windows of the CV 990 aircraft. The telescope is mounted atop one of the "Low Boy" equipment racks provided by NASA for use in this airplane.

Figure 10 is a plan view and shows the area utilization of the window and telescope apertures. The resulting clear aperture is .080 m^2 (124 in^2), the equivalent of a 319 mm (12.6 inch) diameter unblocked telescope. About 75% of the total window area and 90% of the telescope are utilized.

SA-5557-23

FIGURE 8 CELESTRON 14 SCHMIDT-CASSEGRAIN TELESCOPE

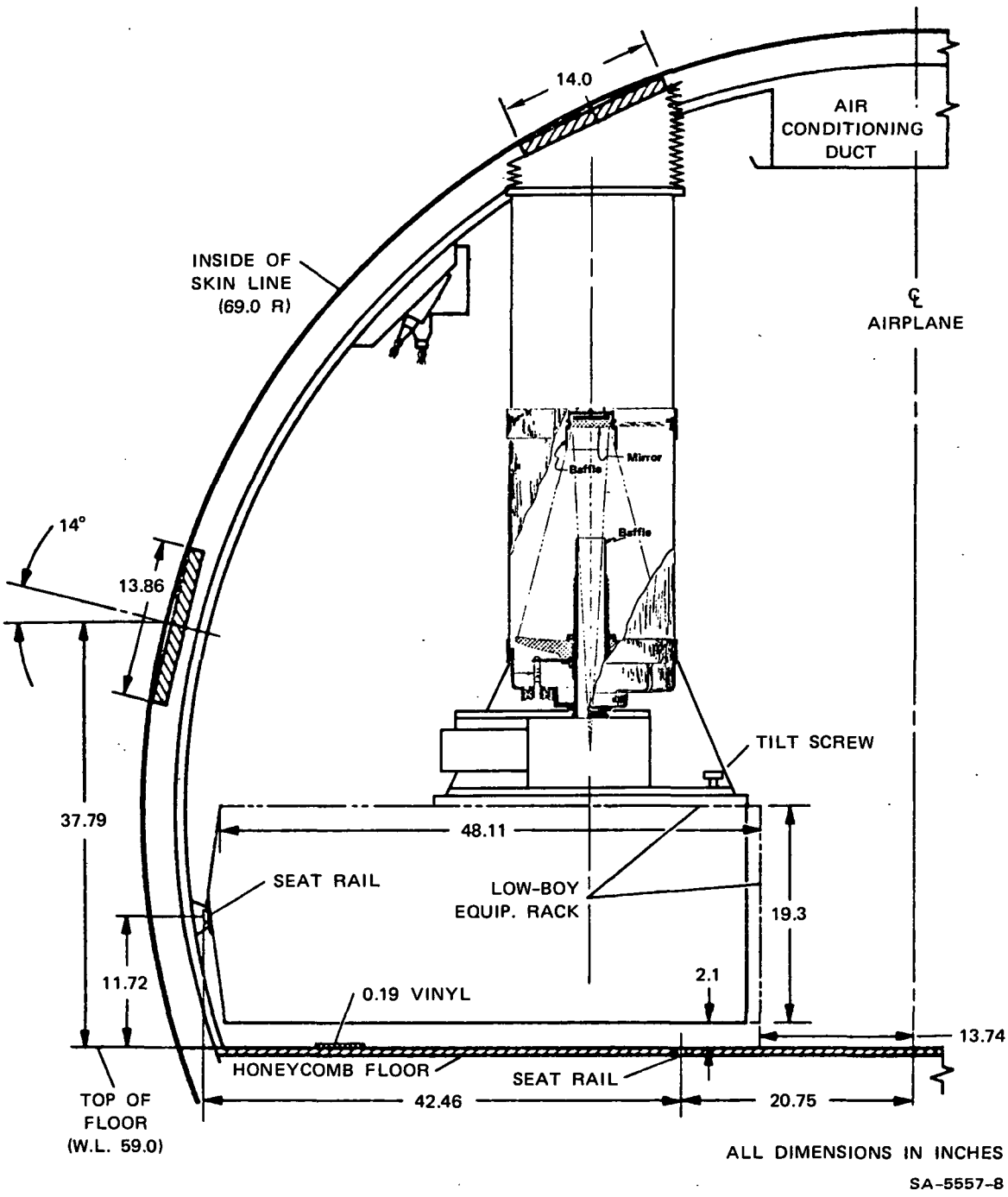

FIGURE 9 MOUNTING LOCATION OF 14-INCH TELESCOPE UNDER 65° WINDOW

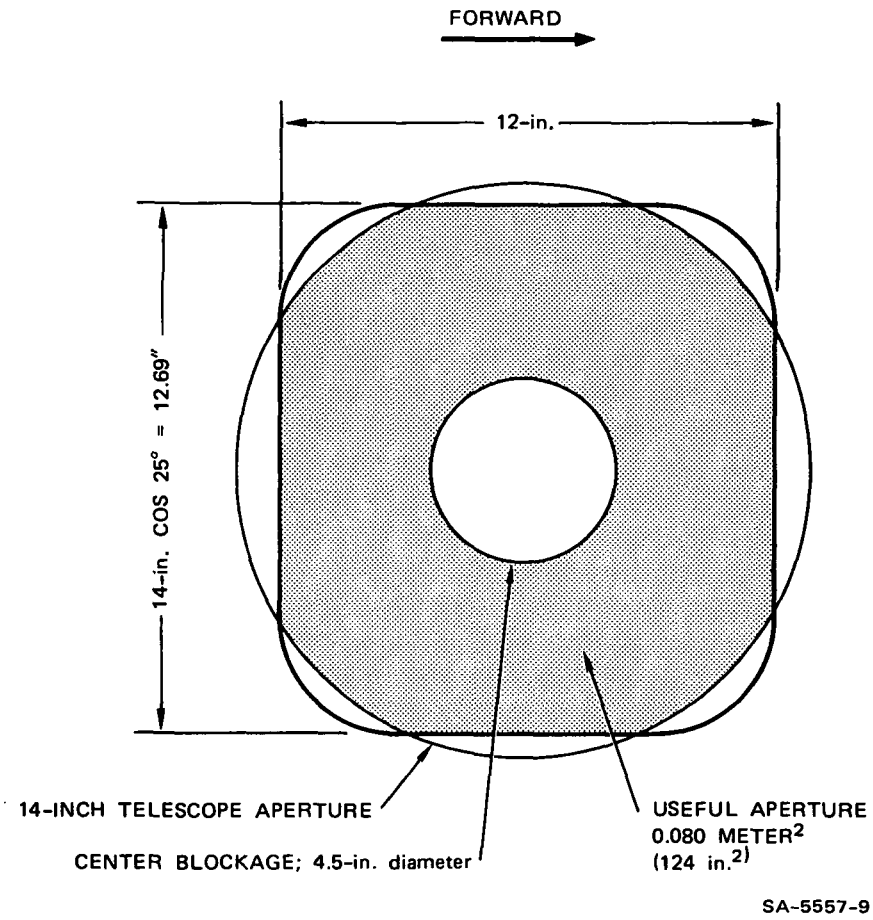

FIGURE 10 PLAN VIEW OF 65° WINDOW AND CELESTRON 14-INCH TELESCOPE

Two different basic designs for focal plane optics have been considered for use with this telescope. Numerous hybrid variations on the same theme are possible in the final detailed design phase.

D. Direct Coupled Receiver

If only a single receiver module is contemplated, the field stop, polarizer, and photomultiplier housing(s) could be rigidly fixed to the rear of the telescope, and screws could be provided to tilt the whole receiver assembly to achieve fine convergence with the transmitter beam.

Figure 11 shows an optical schematic for this rigid-detector option that provides for the narrow band filter, an adjustable field stop, a polarizer, and a quadrant detector assembly for convergence monitoring that will be discussed later. Because of the high effective f/D ratio of the Schmidt Cassegrain telescope, the maximum convergence angle for light rays near the focal plane is small enough (2.6^{o}) that no additional collimation is required to efficiently use narrow band interference filters in the bandwidth range of 5 to 10 Angstroms. The drawing shows a Varian VPM 164 photomultiplier mounted in a thermoelectric cooler (Products for Research, modified Type TE 102). As discussed further in Section V-B, cooling is mandatory for operation at 1.06 microns, but optional at the ruby wavelength. If an uncooled VPM 164 type tube is used, the housing can be a simple cylinder (3" diameter is standard for all SRI lidars) but the converging lens shown would still be required to reduce the beam to fit the small 0.25" recessed photocathode.

Since high efficiency infrared-sensitive photomultipliers require constant cooling, even during storage, the cooler housing should be provided with alignment keys and quick-release fittings to facilitate easy removal from the aircraft during periods when standby power cannot be guaranteed. The design provides for the addition of a second photomultiplier at right angles to the one shown should it be desirable to

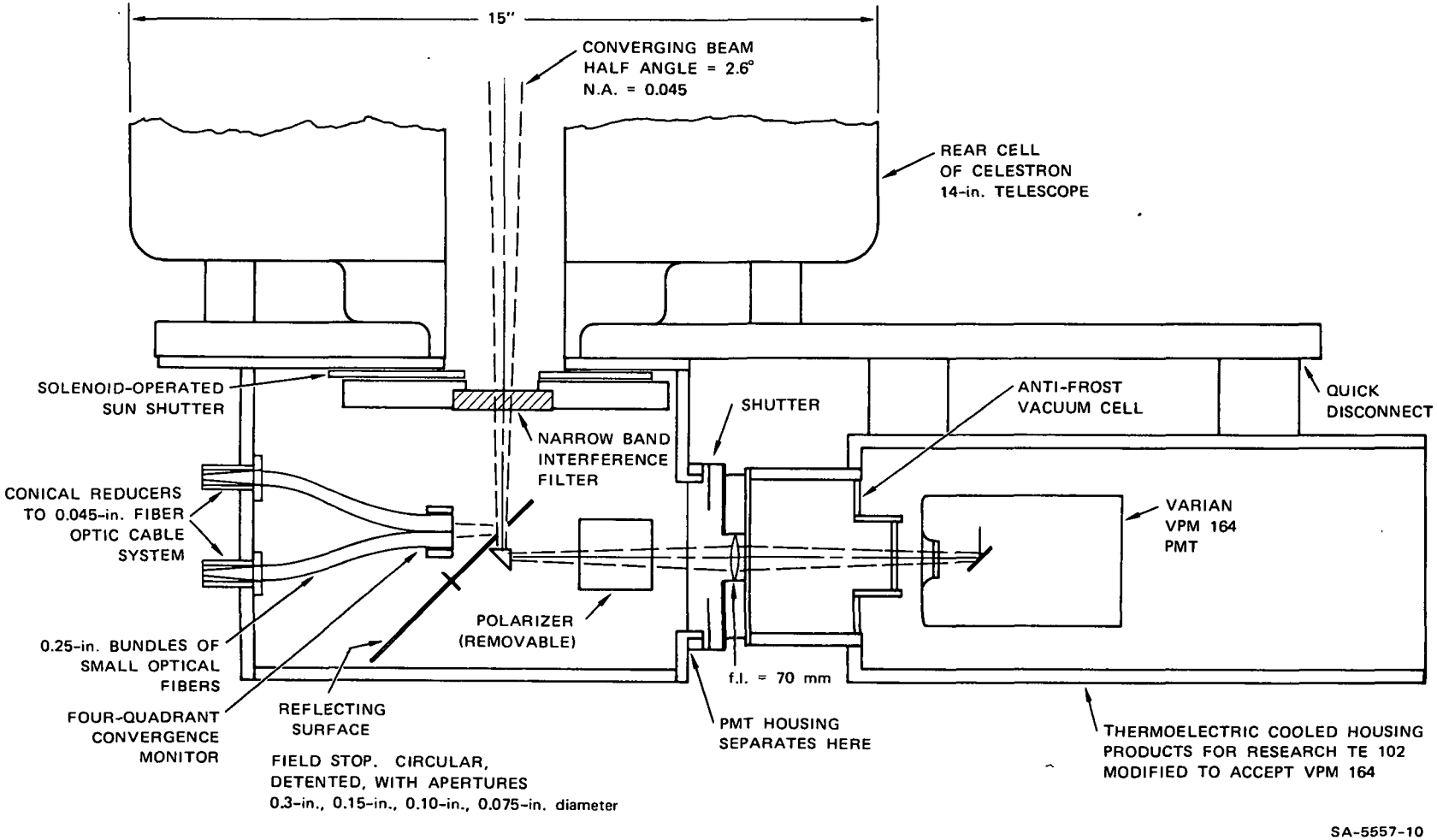

FIGURE 11 OPTICAL SCHEMATIC DIAGRAM FOR DIRECT-COUPLED RECEIVER

conduct experiments that require simultaneous monitoring of both polarizations of the lidar return. Angular adjustment of the polarization plane relative to the aircraft (to minimize the sky return) would require rotation of the entire telescope-detector assembly.

Note that this design, as shown, is not amenable to two-wavelength operation since everything but a single narrow wavelength band is rejected as a first step in the optical signal processing. The simplest option for two-wavelength operation would be to use two separate receivers, one for each wavelength. While that approach would not make maximum use of the available total collection aperture, it might be preferable to a more complex dichroic beam splitting arrangement with its attendant problems of alignment and losses.

One possibility for a two-wavelength version would be to lower everything below the sun shutter in Figure 11 approximately one inch and to insert in the newly created space a 90^{o} dichroic beam splitter, a second narrow-band interference filter followed by a second field stop plate, then a fiber-optic collecting cone and single-strand fiber leading to the alternate-wavelength photomultiplier in a manner analogous to portions of the design to be discussed in the next paragraph.

E. Fiber Optic Coupled Receiver

To permit significant increases in receiving aperture, operation with multiple receiving telescopes has been proposed. These would be optically coupled into a single high quality photomultiplier detector.

For two or perhaps three such separate telescopes, it should be practical to continue to achieve convergence via the direct manual access leveling screw arrangement just discussed. For larger arrays, it will probably be better to provide remotely controllable levelling pads; for example, motor driven screws or thermally-controlled expansion devices.

Another remotely-controllable convergence design has been given some thought and is included here for completeness, though our own current preference would be to resort to its additional cost and complexity only if some basic flaw becomes apparent in the leveling screw arrangement. In this design, illustrated in Figure 12, the "field stop" is the entrance end of a fiber optic light guide that can be moved in the large (3" diameter) image plane of the Celestron telescope by means of a small motor-driven x-y translation table similar to those provided for some microscopes. The entire assembly mounts in a box that clamps to the rear cell of the telescope. The telescope itself could be rigidly mounted, with no requirement for fine adjustment. The dichroic beam splitter could be either a narrow band interference filter, designed for operation at the 45° angle as shown, or a less selective dichroic prism followed by two conventional interference filters. The central large image pickup fiber is surrounded by four quadrant bundles of smaller optical fibers that lead to four separate detectors that are used for convergence monitoring. The main signal fiber is a single strand instead of a bundle in order to avoid the light loss that would otherwise occur because of cladding and air spaces (typical active area of bundles is about 75% - 85%). The effective focal length of the Celestron 14" telescope is 154", so that for a 0.7 miliradian field of view, the fiber entrance aperture (field stop) should have a diameter of about 0.100 inch, which is too large to flex conveniently. A diameter of about 0.020" appears to be more reasonable. Discussions with one leading fiber optic manufacturer, Galileo Electro-Optics Corp., Sturbridge, Massachusetts, indicates that flared, bell-shaped sections remain at the furnance end of a "drawing down" operation. Normally these flared ends are cut off and discarded, but in a custom order, lengths of 0.020" fiber with one end flared to the original cane diameter of 0.187" could be provided. The flared sections could then be cut at the proper point to achieve the desired entrance aperture size.

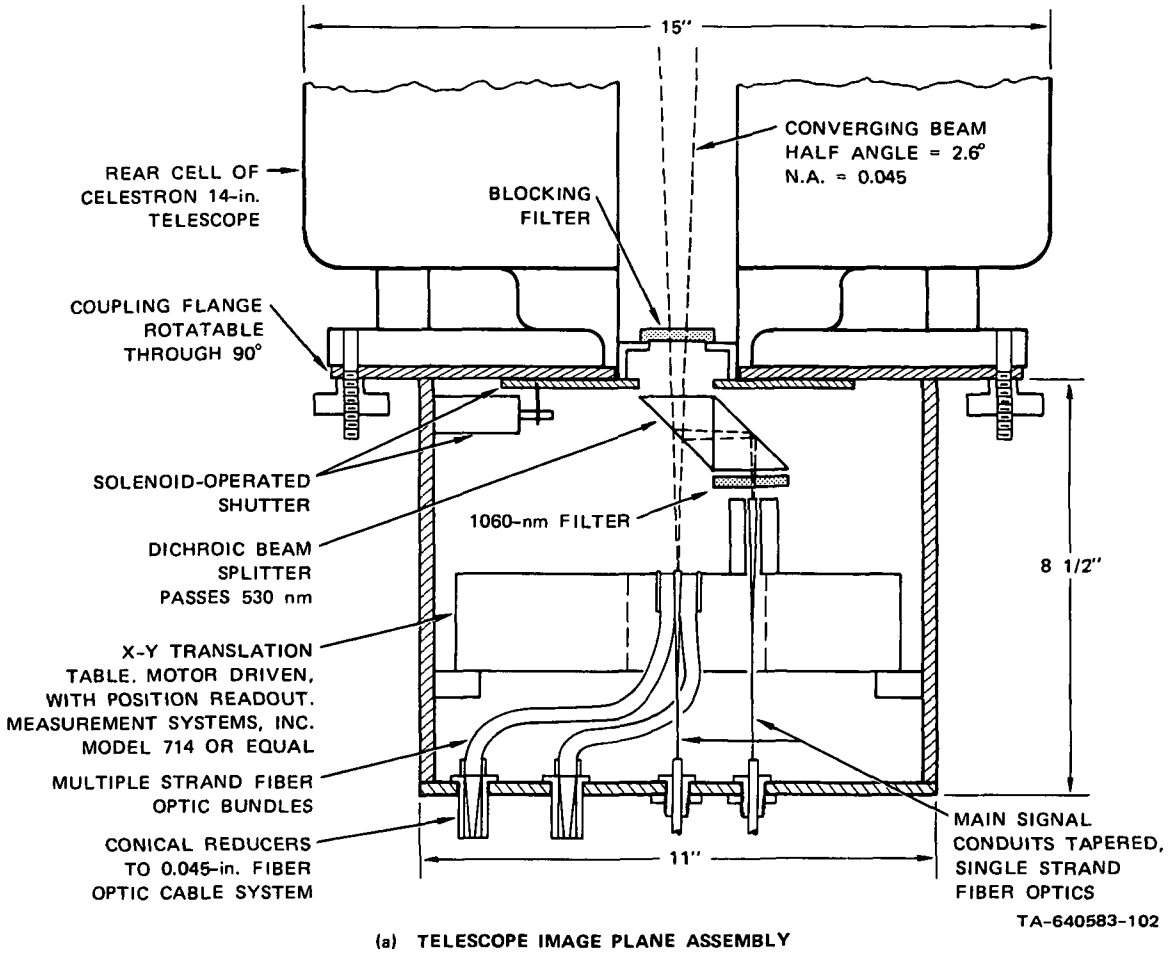

(a) TELESCOPE IMAGE PLANE ASSEMBLY

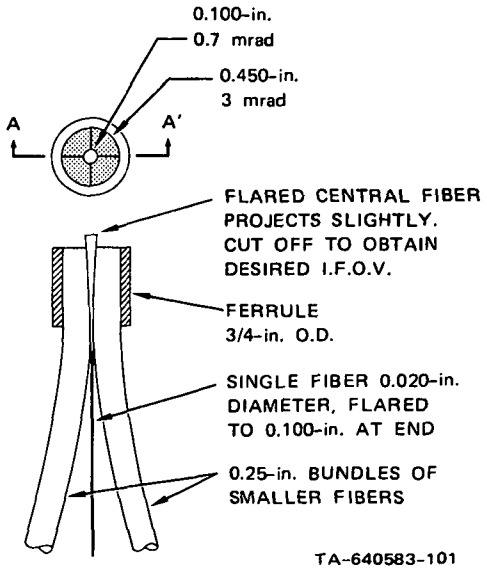

(b) DETAIL OF FIBER OPTIC PICKUP ASSEMBLY

FIGURE 12 OPTICAL SCHEMATIC FOR FIBER OPTIC COUPLED RECEIVER WITH X-Y TRANSLATION TABLE

Light entering a tapered optical guide at an angle θ will emerge at an angle $K\theta$ where K is the ratio of entrance to exit diameters. In our case the maximum entrance angle is 2.6^{o}. Transmission down the guide would then occur with a maximum angle of 13^{o} which is close to the maximum allowed for high transmission fibers. The corresponding numerical aperture, N.A., is sin 13^{o} or 0.22. Available numerical apertures for optical fibers, determined by the refractive indices of the core and clad glasses, run from 0.66 for low quality fibers (0.65 dB/meter) to 0.20 for high quality fibers (0.01 dB/meter).

New Tube Design

The relatively small, deeply recessed photocathode of the VPM-164 tube forces several undesirable optical design compromises that would not be present with a more conventional end-window tube construction, but have been accepted as part of the price of obtaining high quantum efficiency.

As this report is being completed, Varian is announcing a new ruby wavelength high quantum efficiency photomultiplier, VPM-192M, that has a larger (18 mm diameter) photocathode coated on the inside of an end window and will be available at less than one-third the cost of the VPM-164.

For the recessed cathode tubes, relay lenses are required to converge the beam onto the cathode active area, not only for the relatively high dispersion beams exiting from light pipes but even for the relatively low divergence, direct-coupled receiver design of Figure 11. With a larger photocathode having a wider acceptance angle, these relay lenses could be eliminated and a simpler system with higher optical efficiency would result. For fiber-optic coupled options employing cooled housings, the additional losses normally associated with an anti-frost window could be eliminated. The optical fibers could penetrate the cold wall and terminate either near the cathode window or, for highest efficiency could be sealed to the window with an index-matching compound.

Initially, the VPM-192 design will be available only with a GaAs (red sensitive) cathode. The advertised quantum efficiency at 700 nanometers is 10%, compared to 15% for the VPM-164M, but apparently this difference is due not to a technical limitation, but to a current Defense Department security classification that is expected to be relaxed soon.

Varian expects that it will be at least a year before an infrared-sensitive version of this new tube type might be available. For this reason, along with the possibility that further testing of the end-window tube may reveal some limitation peculiar to the lidar application (refer to Section X-A for examples) it would be well to keep the receiver design flexible enough to be able to accomodate either tube type.

F. Convergence Monitoring

Both of the 14-inch receiver design options employ a specially fabricated four-quadrant grouping of optical fibers surrounding the field stop that defines the main field of view. With perfect transmitter/receiver alignment (convergence), all of the returning laser light will be focused through the field stop and on to the main signal detector, either immediately for the case of the direct-coupled receiver or via a light pipe for the case of the fiber-optic coupled receiver. If the convergence is not optimum, a portion of the focused laser return will fall on one or two of the four pie-shaped fiber optic bundles surrounding the central field stop. The magnitude and the direction of the misconvergence can be monitored by an auxiliary detection system at the exit end of these cables. It is anticipated that any convergence drift will be slow enough and infrequent enough that one detector and monitoring circuit could be time-shared among several quadrants in several telescopes. For example, Figure 13 shows a possible arrangement for a four-telescope receiving array. The detector should probably still be a photomultiplier tube, but it could be a more common and less expensive type than that proposed

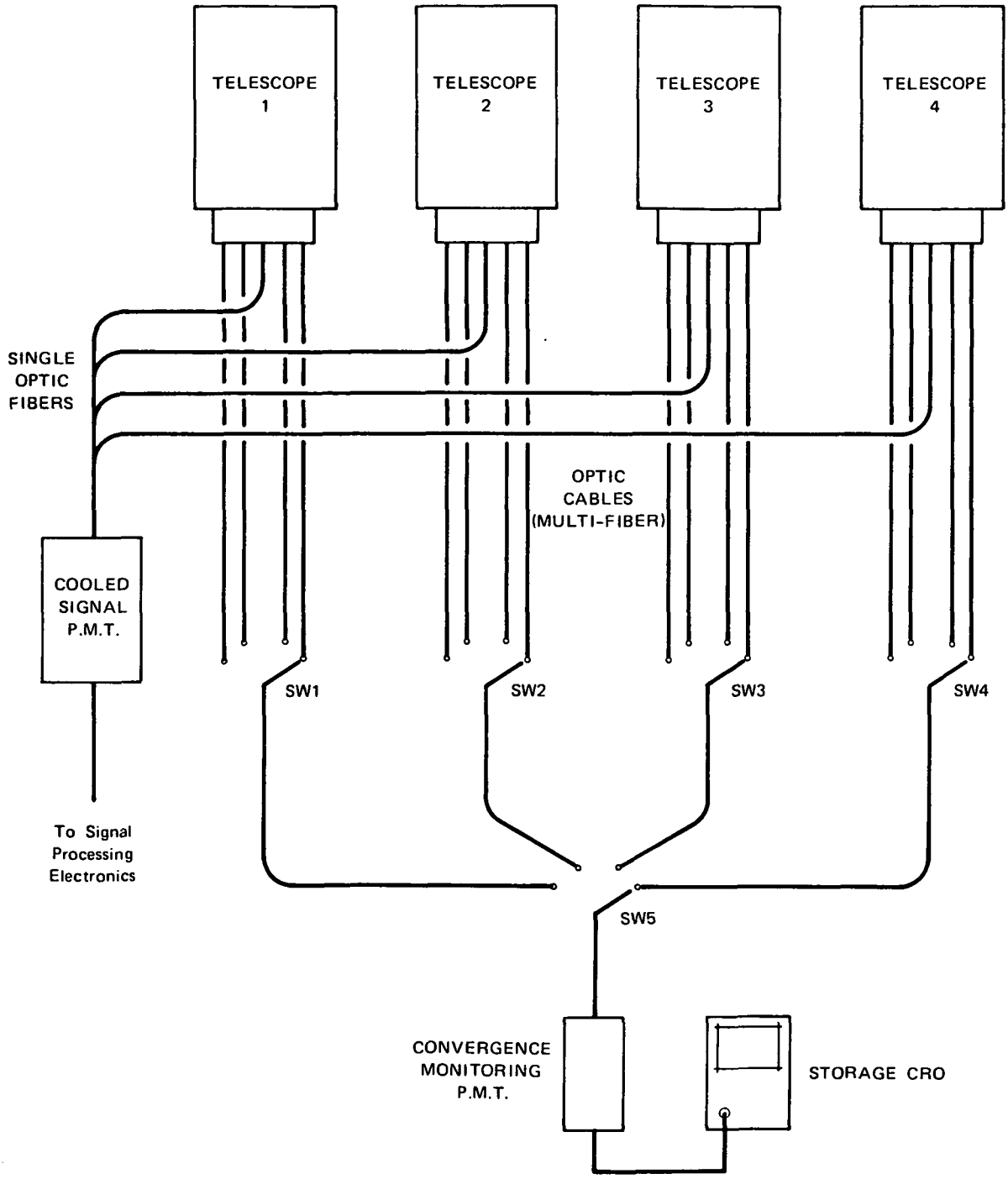

NOTE: SW1 through SW5 are 4-position fiber optic selector switches fabricated from electrical switch kit components.

TA-640583-100

FIGURE 13 OPTICAL CABLE DIAGRAM, MULTIPLE TELESCOPE LIDAR RECEIVER

for the main signal. An RCA 7265, with a quantum efficiency of .02, for example, would be quite adequate for the ruby wavelength. For operation at 1.06 microns, this might be a place for a silicon avalanche diode detector.

For monitoring the convergence detector output, a storage oscilloscope, Tektronix 7623, Hewlett-Packard 1741A, or equivalent, is proposed. This scope would also be useful for field testing of the main signal channels in case of trouble with the digital data acquisition system.

The manually-operated fiber optic selector switches, the storage oscilloscope, and actuator controls for the motor-driven convergence assemblies would be grouped together. For the single-telescope, direct-coupled design, the oscilloscope would need to be located within arm's length of the telescope tilting screws. During normal operation, the operator would occasionally cycle through the several convergence monitoring channels, noting any departures from the expected waveforms, and making any required convergence corrections. With proper orientation of the quadrants, two that monitor in the direction toward the transmitter should always display strong backscatter at close ranges, that is, before the region of optimum convergence. Monitoring on these two waveforms may prove to be a more sensitive indicator of convergence than watching for small signals in all channels at ranges where best convergence is desired.

A fine point of difference between the two receiver designs is that in the direct-coupled version a choice of several different field stop sizes is provided (by rotating the mirrored plate) and any laser light that does not penetrate through the hole is reflected onto the convergence monitoring sectors. For the fiber optic version, shown in Figure 12, the field of view is determined by the entrance diameter of the central fiber and is not easily changed. The field could be reduced by adding a small anular cap to the end of the fiber, but then there would be a corresponding anular dead space between the signal channel and the convergence channels.

G. Optical Transmission Factors

Optical transmission factors used in the system design considerations are listed in Table IV. The table breaks down the components of the approximate efficiency figure (exclusive of mechanical blockage) of 0.25 used in many of the calculations; that is, 0.5 for the narrow band filter and 0.5 for all other transmission losses.

Contrary to inferences in the CV-990 Experimenters' Handbook, the optical data available from NASA/Ames about the special optical windows provided for the aircraft are very meager. However, as a part of a lidar experiment flown on the CV-990 in 1969 for the BOMEX expedition, J. Oblanas of SRI made transmission measurements and laser damage checks at the ruby wavelength on Borosilicate Crown, Pyrex (also a Borosilicate) and Soda-Lime glass window blanks borrowed from Ames. Of these three samples, the Borosilicate crown was the best, having measured one-way transmission of 0.96 for both polarizations at the working incidence angle of 25^{o}. Handbook curves indicate that the transmission factor at 1.06 micrometers should not be measurably different from that at the ruby wavelength (0.694 μm).

Table IV

OPTICAL TRANSMISSION LOSS FACTORS USEFUL IN COMPUTING RECEIVER EFFICIENCY

Component	Wavelength			
	0.694μm		1.06μm	
	Normal	Possible (a)	Normal	Possible
990 window	0.05[b]	0.02	0.06	0.02
Correction plate	0.09	0.02	0.09	0.02
Primary reflector	0.06	0.03	0.06	0.03
Secondary reflector	0.06	0.03	0.06	0.03
Light pipe entrance loss	0.06	0.02	- - - -	- - - -
Light pipe transmission loss (1 m, Galite 2000)	0.08	- - - -	0.08	- - - -
Light pipe exit loss	0.06	0.02	0.06	0.02
Microscope objective	0.05	0.00	- - - -	- - - -
PMT window (sapphire)	0.04	- - - -	- - - -	- - - -
Polarizer	0.05	0.03	0.05	0.03
N.B. filter	0.50	- - - -	0.50	- - - -

[a] With A.R. coating and/or special surface treatment.

[b] Uncoated borosilicate glass 1-inch thick. SRI measurements at 0.694 μm by Oblanas, 1969 (unpublished).

VI BEAMWIDTH/CONVERGENCE RELATIONS

When the lidar receiver is located some distance from the transmitter, as proposed here, there is a need to consider the effect of transmitter and receiver beamwidths on the ranges over which useful convergence (overlap) of the two beams can be maintained. If background ambient lighting could be ignored, there would be no problem. The receiver field of view could be enlarged as necessary to always include the transmitted beam. However, for all flights coincident with SAM-II observations, there will be a need to control the sky noise contribution by minimizing the receiver field of view.

Section VI presents relationships among beamwidths, transmitter-receiver spacings, and operating ranges in a form intended to expedite the evaluation of trade-offs among these parameters on system performance for the several lidar options proposed. The geometry is illustrated in Figure 14, where the region between R_{min} and R_{max} is where the two beams are fully converged; that is, share a common volume. From this figure, the following simple relationships can be derived:

$$R_{min} = \frac{S}{\Phi + \frac{\theta_R - \theta_T}{2}} \tag{6}$$

$$R_{max} = \frac{S}{\Phi - \frac{\theta_R - \theta_T}{2}} \tag{7}$$

where R_{min} is the closest range for full convergence, in kilometers

R_{max} is the greatest range for full convergence, in kilometers

$\theta_{R/2}$ and $\theta_{T/2}$ are the receiver and transmitter beam half angles, respectively, in miliradians.

Φ is the toe-in angle between beam centers, in miliradians, and

S is the transmitter-receiver separation, in meters.

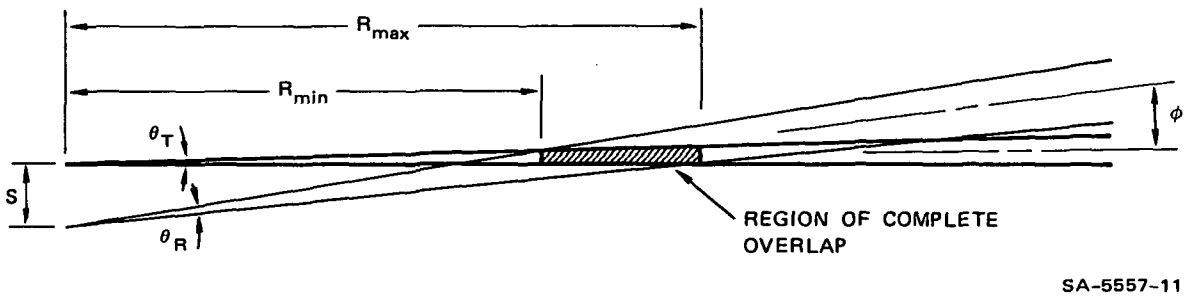

FIGURE 14 BEAM OVERLAP GEOMETRY FOR SEPARATED RECEIVER AND TRANSMITTER

These two equations, and the ratio between them, are plotted in Figures 15, 16, and 17 for angles and spacings of interest for the CV 990 aircraft installation. Location of the available upward-looking windows are shown in the plan view of the aircraft, Figure 18. In addition to those shown, we understand that the aircraft now has two 65° windows separated by only 19" (0.5 meter).

From Figures 15, 16, and 17, the following observations can be made that are useful in system design and adjustment:

- For any spacing S greater than zero, a critical parameter is $\theta_R - \theta_T$, the angle by which the receiver beamwidth exceeds the transmitted beamwidth. If $\theta_R = \theta_T$, full convergence can occur at only one range point.

- R_{max}/R_{min} gets infinitely large if toe-in $\emptyset$ is not larger than $\frac{\theta_R - \theta_T}{2}$. Beyond that point, we loose rapidly in convergence range as $\emptyset$ is increased in an effort to reduce R_{min}.

- Toe-in normally should be adjusted to yield R_{min} no smaller than required by the experiment. At the same time, $\frac{\theta_R - \theta_T}{2}$ can be increased until the desired R_{max} is reached, or until the background sky noise becomes limiting, whichever comes first.

For a one or two receiver installation in the CV 990, S will be on the order of 1 meter. If an R_{min} of 4 km can be accepted, a value of $\theta_R - \theta_T$ of .25 miliradian appears reasonable, and this is the value that has been assumed in most of the trial calculations.

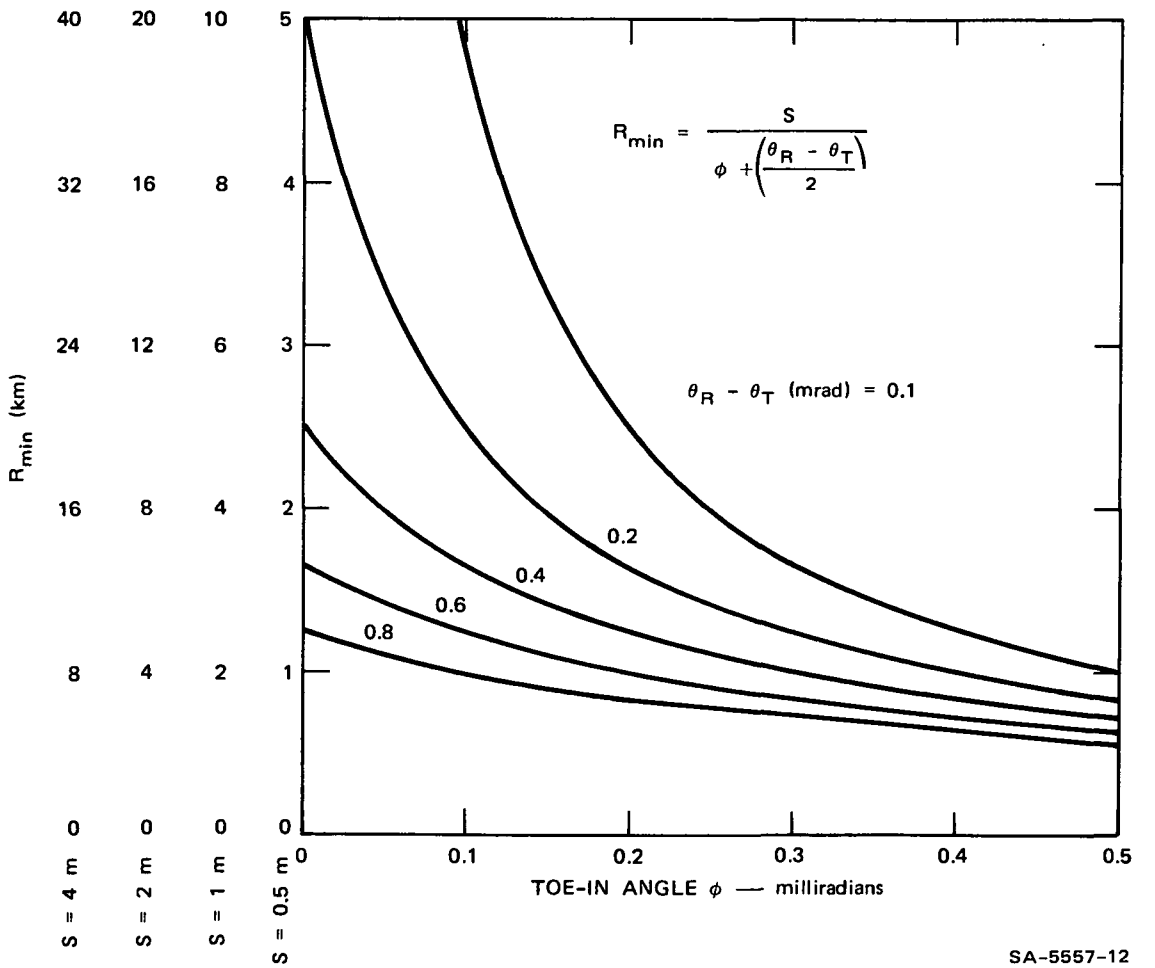

FIGURE 15 MINIMUM CONVERGENCE RANGE VERSUS TOE-IN ANGLE

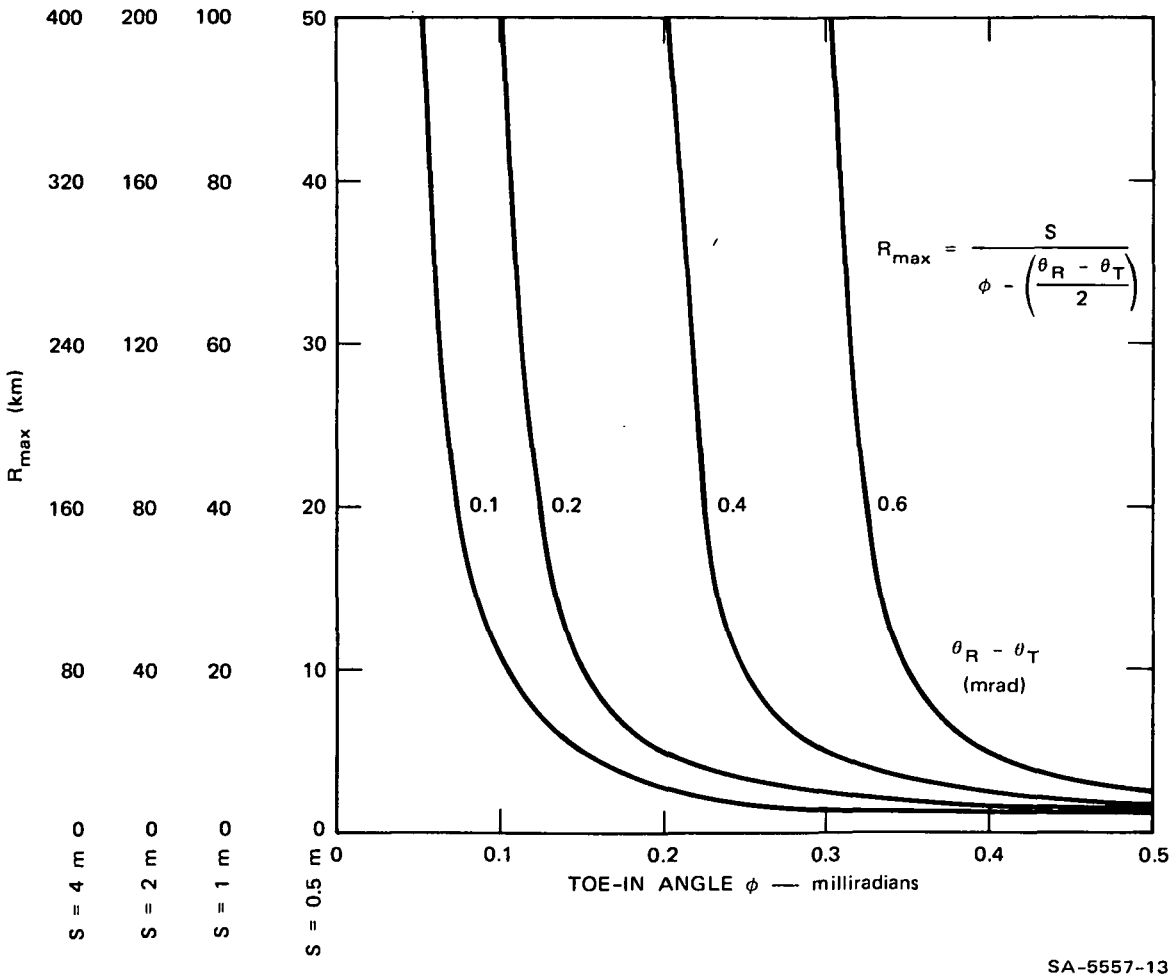

FIGURE 16 MAXIMUM CONVERGENCE RANGE VERSUS TOE-IN ANGLE

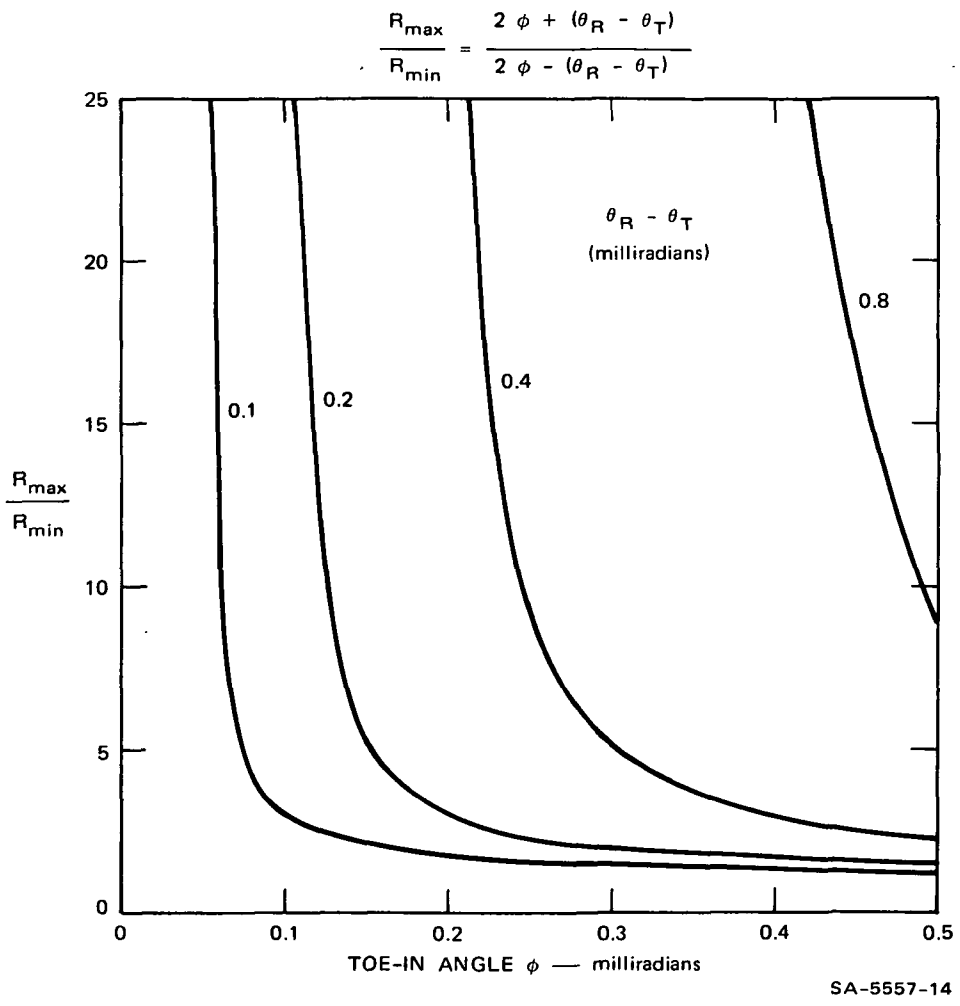

FIGURE 17 CONVERGENCE RANGE VERSUS TOE-IN ANGLE

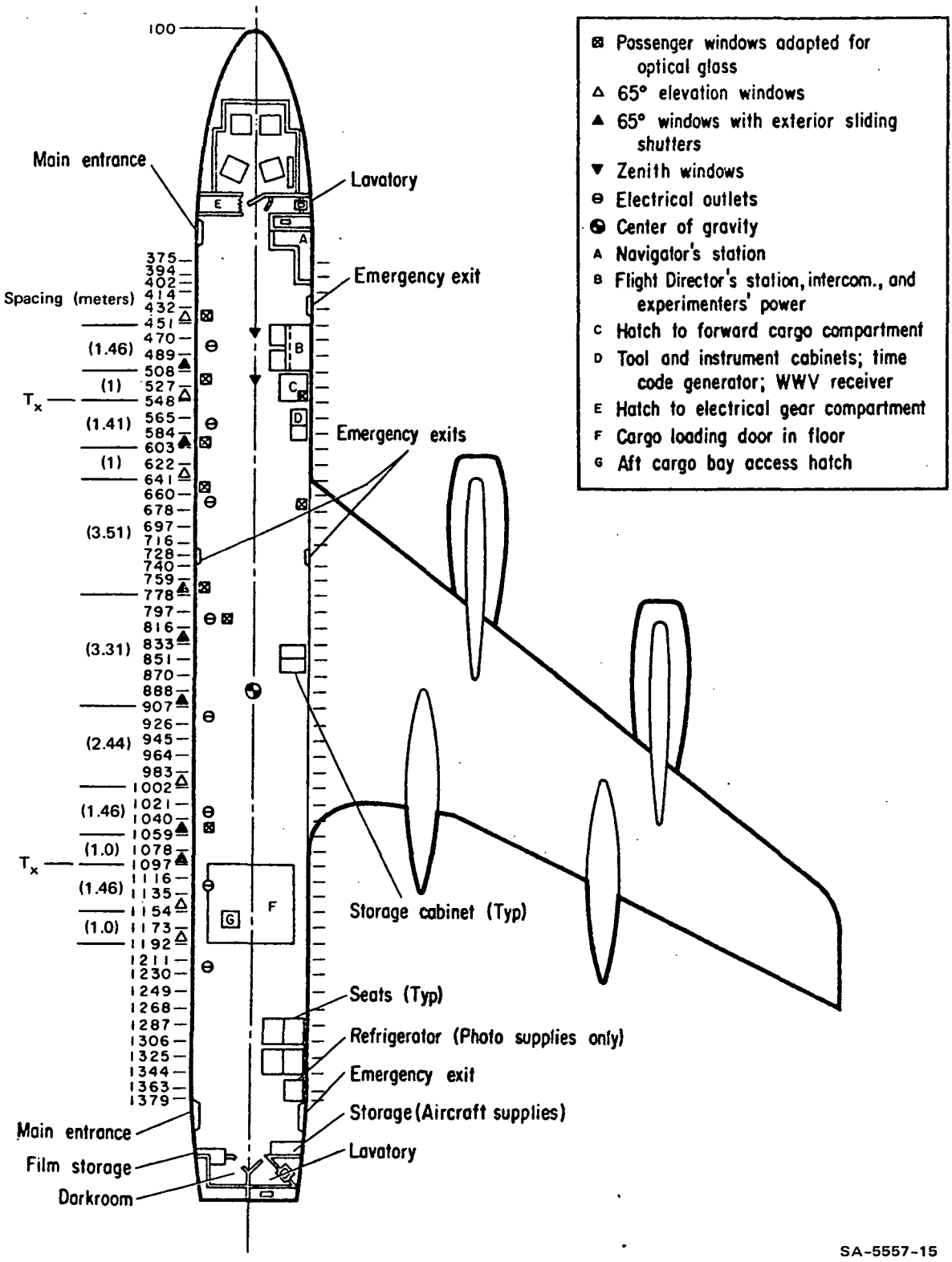

FIGURE 18 GENERAL CABIN LAYOUT OF NASA CV 990

"Belt frames" are numbered by their distance in inches with the nose tip being referenced at 100. Two possible locations for a central transmitter in a four-receiver system are shown, at belt stations 548 and 1097.

"Page missing from available version"

p. 54

VII DATA PROCESSING AND RECORDING

As is evident from Figure 2, the signal levels expected for altitudes of interest will vary from one photoelectron count per several hundred microseconds for altitudes above about 70-80 km up to tens of thousands of counts per microsecond for the region a few kilometers above the aircraft; that is for altitudes in the region of 15 km. The weaker returns are clearly in the realm of "photon counting" while the stronger ones are well above rates that can be counted by conventional digital techniques and where analog recording conventionally has been employed. Midway between these two extremes is an approximately two decade range (one to 100 pulses per microsecond) that is in the transition range where the use of conventional approaches to either pulse counting or analog recording encounters practical problems. Further, these problems occur in altitudes of particular importance to the SAM II aerosol measurement program and where it would be desirable to avoid courting still more troubles by switching scales or recording procedures. The proposed data recording system attempts to circumvent these problems by employing a pulse integration scheme that operates in a single mode not only through the critical 1-100 count/microsecond range but over at least one decade on either side of that range by employing a reliable, repeatable and high precision scale change method. The basic procedure is illustrated in Figure 19.

A storage capacitor, C, is provided to accumulate charge delivered from the photomultiplier anode. Each photoelectron ejected from the photocathode will result in a short burst (approximately 10 ns due to transit time dispersion) of G electrons out of the anode, where G is the operating gain of the PMT. G and the size of the storage capacitor will be chosen so that the capacitor voltage, $V_C = Q/C$, will be at

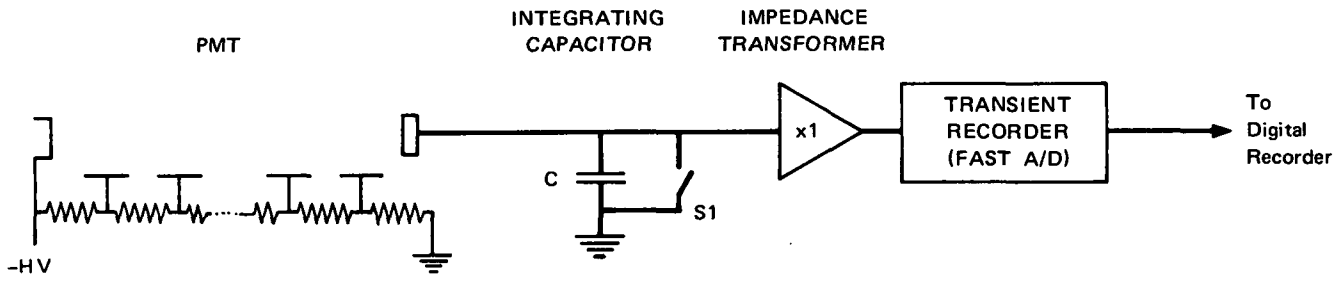

(a) CIRCUIT BLOCK DIAGRAM

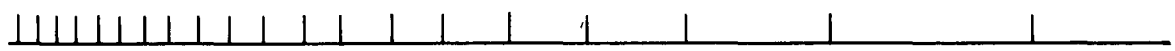

(b) DECAYING ANODE PULSE TRAIN

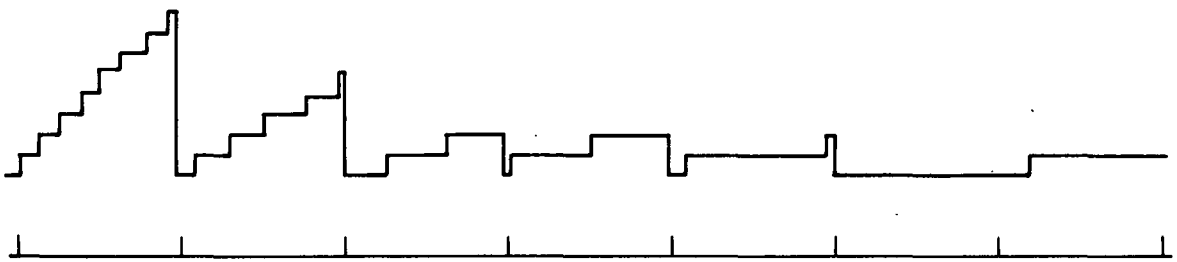

(c) INTEGRATOR VOLTAGE (SAMPLED THEN DISCHARGED AT TIMES SHOWN)

SA-5557-16

FIGURE 19 ANODE PULSE INTEGRATOR

least as large as the least count increment on the Biomation transient recorder. At the end of each range integration period, the Biomation unit will sample the accumulated capacitor voltage and the capacitor will then be immediately discharged to zero by brief (< 50 ns $\pm$ 57%) closure of semiconductor switch S1. The switch closure time will be dead time during which integration will be inactive, but this can be compensated for as a scale factor in later processing and is considered preferable to the alternative of providing low level switching to alternate between two storage capacitors, one being charged while the other is discharged.

Ideally one would like to use a pulse amplitude discriminator and a standardized pulse generator between the anode and the integrating capacitor. This is not practical because of the difficulty in separating closely spaced and partially overlapping pulses. As an alternative we specify a photomultiplier designed and tested to have a narrow pulse amplitude distribution for single photon events at the cathode. Figure 20 shows Varian measurements of pulse distributions for the VPM 164 series tubes with standard and galium phosphide first dynodes. The superiority of the galium phosphide dynode is clearly evident.

Full scale for the Biomation recorder is 256 counts (8 bits), and the input scale factors cannot be changed during a transient acquisition cycle. Additional dynamic range can be achieved by changing the range integration period, the amount of stored charge per photon (varying PMT gain G), or both. Varying the integration time appears conceptually more attractive than varying the gain, because pairs of time gates having "on" periods in precisely defined ratios can be generated by digital countdown from a highly stable clock oscillator. However the concept encounters practical limitations that prevent it from being extended indefinitely in either direction along the time scale. Obstacles in the fast direction are minimum time in which the storage capacitor can be discharged and

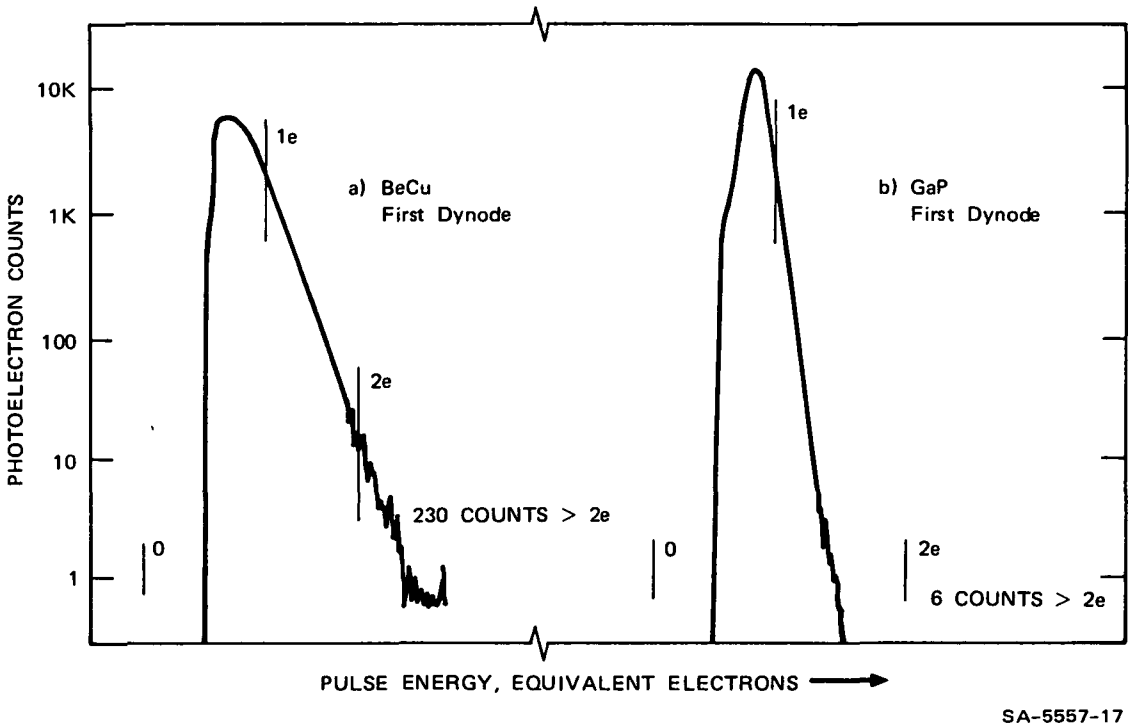

FIGURE 20 PULSE HEIGHT DISTRIBUTION, VPM 164 PHOTOMULTIPLIER TUBE

the excessive number of range storage bins required to cover the altitude ranges of interest. In the slow direction, the limit is set by the longest tolerable range integration period. The standard Biomation 8100 provides for switching between two pre-programmed and digitally derived sample intervals (range intervals) once during each acquisition. If necessary, more complete control could be obtained by supplying an external variable rate clock but this does not appear to be required, at least initially.

The gain of the PMT can be controlled conveniently over at least two decades by modulating selected dynodes in a manner that has been used successfully in the three most recent SRI lidar designs and is described by Allen and Evans, (1972). We believe that essentially the same procedure can be applied to the Varian PMTs and that with the provision of suitable built-in test facilities and operating techniques,* the gain-switching precision can be maintained to better than 1%.

A key point is to provide some flexibility in tailoring the gain switching points to the needs of a particular experiment without providing so many options that system calibration or data reduction becomes unduly complex.

The proposed dumping of the integration capacitor at the end of each increment (sometimes called "box car" integration) circumvents a practical problem that frequently occurs in choosing the amount of video filtering to be used before display or recording of analog lidar waveforms. If the bandwidth of the filter is made small enough that the quantum

---

*For example, a gain switch of 10x could be checked by providing two light pulses, feedback stabilized to differ in amplitude by 10x, timed to occur before and after the gain switch, and of sufficient amplitude to produce nearly full scale response in the Biomation digitizer. The pulses could be generated by light emitting diodes and fiber-optic coupled into the PMT in an occasional dummy recording cycle interleaved between normal lidar firings. Digital readout of the stored Biomation values for the two test range cells would provide both a check and a record of gain-switching performance.

noise fluctuations are averaged to yield a clean (that is, not fuzzy) trace, the time constant will be long enough that the observed amplitude in any particular range cell is necessarily affected by the signal return level in several preceding range cells. While this effect could possibly be compensated for by digital signal processing, it would require additional programming and processing time that is not needed when the slate is wiped clean at the beginning of each range cell.

The procedure just outlined maintains all data recording in a linear mode, avoiding the need for questions about the accuracy of a logarithmic response amplifier, and simplifying the arithmetic required to achieve pulse integration over various combinations of shot numbers and range integration periods.

As an example, consider the case of the single 14" receiver in a 1 joule ruby system. Expected photoelectron counts vs altitude are taken from Figure 2. Assume that 0.5 microsecond (0.075 km) range increments will be used for the region between the aircraft and 40 km altitude. This requires 400 range bins (200 microseconds).

From 40 to 90 km elevation, 5 microsecond (0.75 km) range bins will be used. This requires an additional 67 range bins covering 333 microseconds in time.

For these conditions, a barely acceptable recording gamut might be obtained with the one rate change plus one gain change. The PMT rests in a very low gain mode ($G < 10^4$) in order to prevent anode current overload from bright sky background during the interpulse periods. Approximately 33 microseconds following emission of the laser pulse, the PMT gain would be increased to $G = 10^5$, which corresponds to a Biomation range of 10 to 2560 counts per range increment or 20 to 5120 counts per microsecond. From Figure 3 it can be seen that for a normal Rayleigh atmosphere, the system should emerge from saturation at about H = 16 km and be within recording

range out to about H = 31 km. To provide some margin for signal variation, the PMT gain might be switched to G = 10^6 at an elevation corresponding to 100 pulses per microsecond, approximately 26 kilometers. The Biomation recording range would then cover 2 to 512 counts/μ sec. which would be adequate to cover the range out to H = 40 km, at which point the sampling rate would be lowered by a factor of ten to provide another decade increase in the input signal level to the Biomation. This recording mode would be good up to 90 km, or whatever altitude recording limit might be established.

Should it become necessary to record data closer to the aircraft, an additional segment employing still lower PMT gain could be employed ahead of the sequence just described. In any case, provision should be made to log the pertinent data about gain settings, gain transfer range points, and aircraft altitude on the data tape, either as header information at the beginning of each record (preferably) or as a header record at the beginning of each data file.

For operations up to the one shot per second (maximum rate of the Mark IX lidar) it will be practical to keep a magnetic tape record of each lidar shot, leaving complete freedom of choice for any later multi-shot integration procedures. Each 467-sample shot, together with a time label, a transmitted energy reading, and other supplementary data could be recorded in the relatively extravagant but convenient scientific (floating point) notation in 2048 8-bit bytes, using the PDP-11 format.

A 600 foot reel of 800 bpi tape would hold 36 minutes of recording and either a 4 cm DECTAPE or an 8 cm floppy disc would hold enough data (> 2 min) to permit the main tape drive to be rewound and reloaded.

For operation with a high prf (30 pps) system, the same or very similar pulse counting procedures, range bins, and recording format would be applicable. It would be desirable, however, to perform real-time integration in the computer, both to conserve recording space and to

provide for more meaningful display and interpretation of the data during the experiment. A reasonable arrangement would be to integrate 100 shots (3 seconds) before outputting the summed data to tape, again as a 1024 byte record of 512 floating point numbers. Each 600 foot tape reel would then last for 1.8 hours. Unless the laser can be shown to be inherently free from double pulsing problems, some form of alarm to signal this defect would be essential.

Hardware

The data processing and recording hardware required to perform these functions is illustrated in Figures 21 and 22.

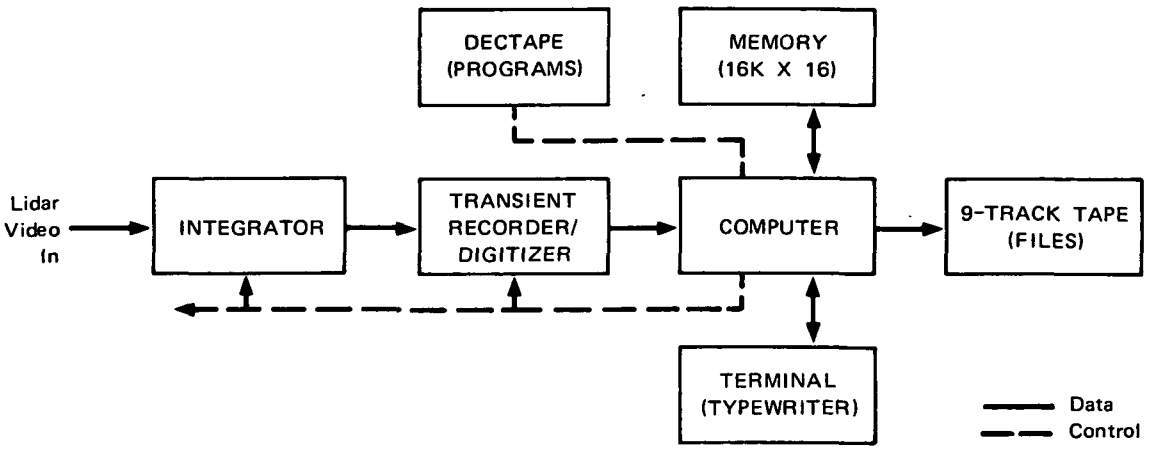

(a) **BLOCK DIAGRAM**

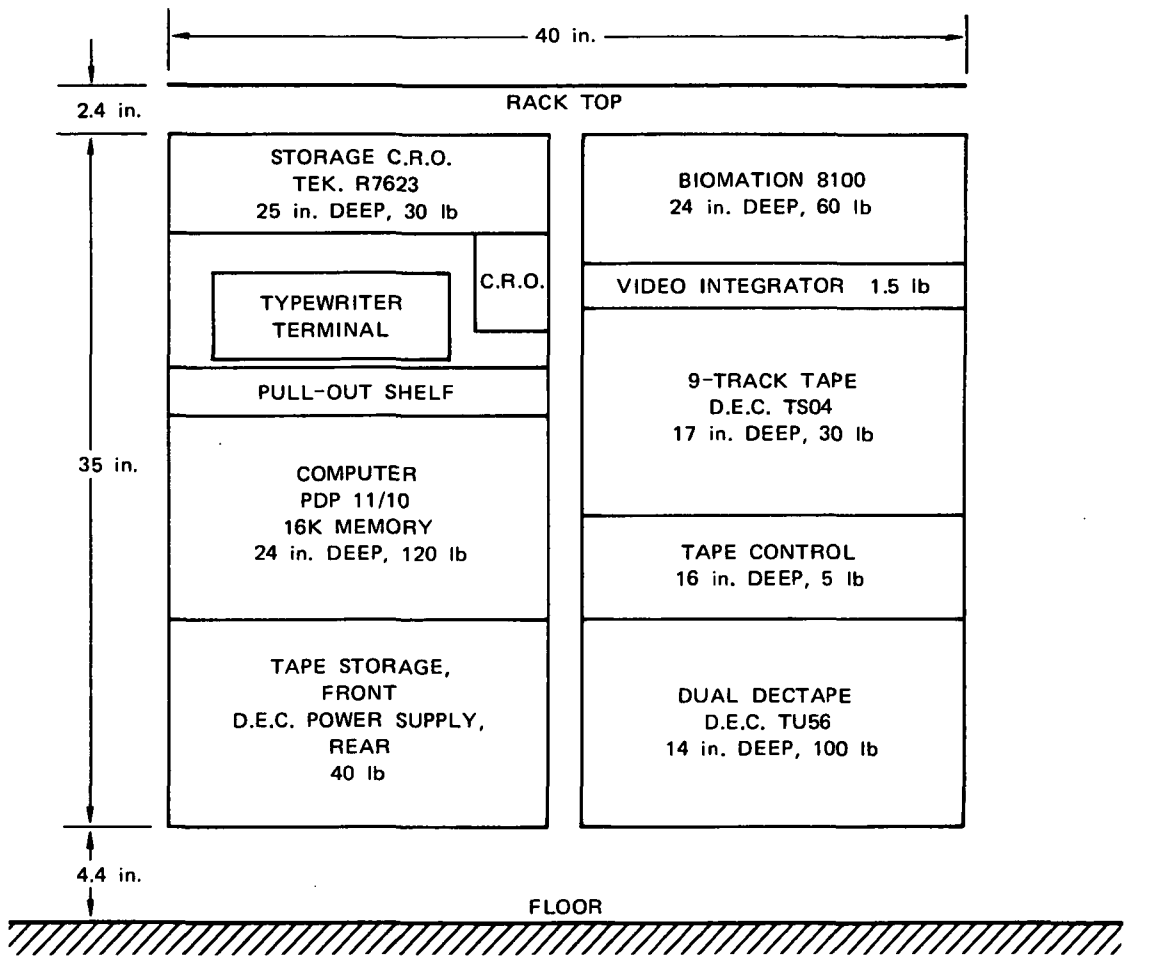

(b) **PHYSICAL ARRANGEMENT AND WEIGHTS**

SA-5557-18

FIGURE 21 AIRBORNE DATA PROCESSING AND RECORDING SYSTEM EMPLOYING MARK IX LIDAR COMPONENTS PLUS 9-TRACK TAPE

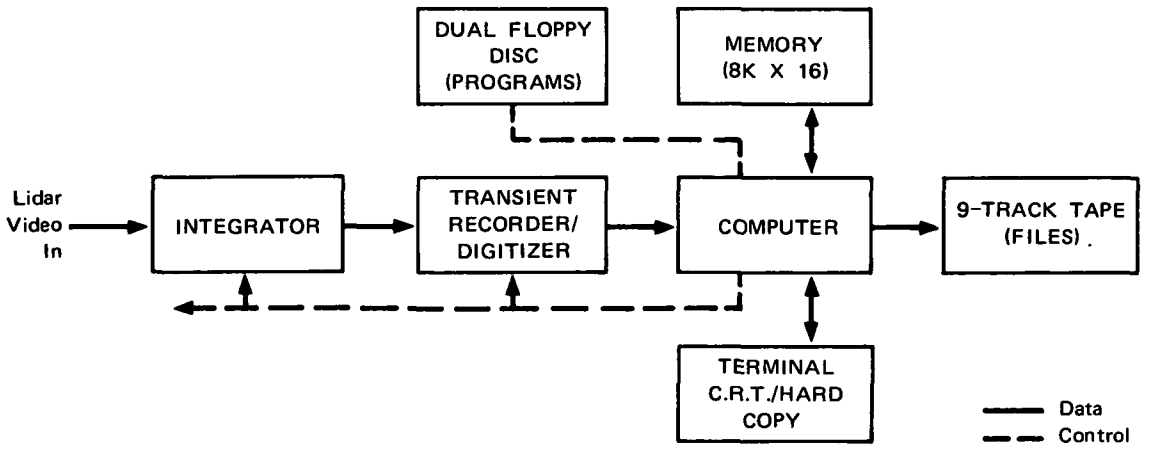

(a) BLOCK DIAGRAM

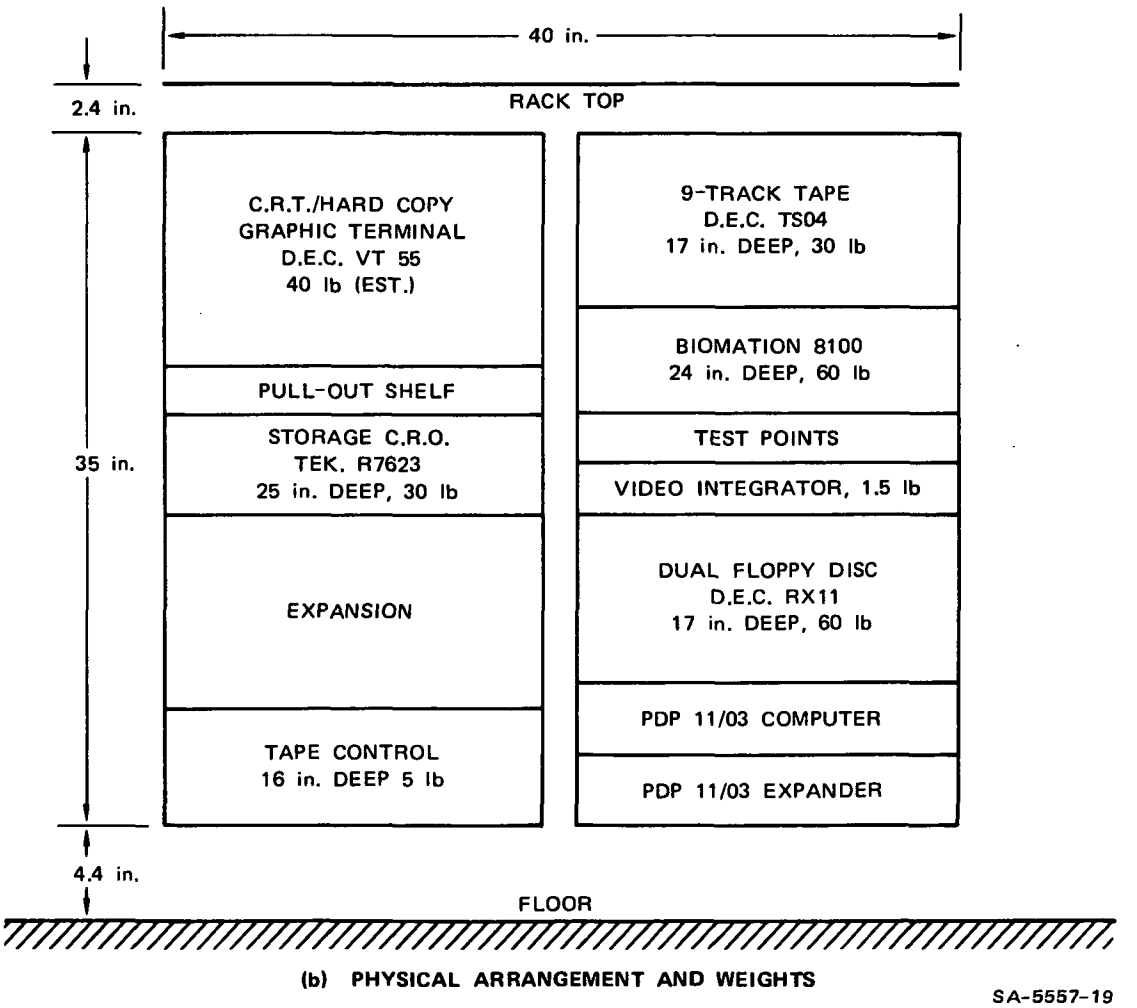

(b) PHYSICAL ARRANGEMENT AND WEIGHTS

SA-5557-19

FIGURE 22 DEDICATED AIRBORNE DATA PROCESSING AND RECORDING SYSTEM

VIII INSTALLATION OF MARK IX LIDAR IN CV 990 AIRCRAFT

A. Existing Mark IX System

Table V lists technical specifications for the current SRI general-purpose atmospheric lidar system, the Mark IX. Figure 23 shows two general views of the equipment, as normally maintained in a self-contained van, including motor-generator power units. Not shown in the picture is the digital data acquisition, which occupies another full equipment rack. Of the units pictured in Figure 23(b), only five would be required to operate the transmitter in an aircraft. Weights, dimensions, and power consumption for these units are given in Table VI. Figure 24 shows details of the lidar head assembly.

1. Mechanical

Figure 25 shows a special mounting pedestal suitable for mounting the Mark IX lidar head for vertical pointing through a 65° window of the NASA CV 990. The design is well within all of the stress limits specified in the NASA Experimenters' Handbook (1975) and should be rigid enough to maintain covergence in a multireceiver system while flying in non-turbulent air. The main frame is a welded and/or bolted assembly of aluminum channel that clamps to the floor and side seat tracks. A two-column yoke is rotatable around a central pivot, but normally would be firmly bolted to the frame in either of two possible 90° orientations, to provide transmitter polarization either parallel or perpendicular to the flight line as discussed in Section III B-4, the fore and aft mode should be prefered for SAM II missions. In addition, the head can be installed in the yoke in either of two 180° options to permit

Table V

MARK IX LIDAR SPECIFICATIONS

Transmitter	
Laser rod	Ruby (3/8 x 3 inches)
Wavelength, A	6943.0 ± 0.4
Beamwidth, mrad	< 1
Optics	4-to-1 Galilean beam expander and 2-inch mirror coaxial with receiver telescope
Pulse energy	1.0
Pulse length, ns	30
Q-switch	Pockels cell
Maximum PRF, pulses/min	60
Cavity cooling	Refrigerated water
Receiver	
Optics	Newtonian reflector (6 inches)
Field of view, mrad	1.0 to 5.5
Predetection filter passband width, A	3 to 5 (thermally controlled)
Detector	RCA 7265 PMT (S-20 photocathode)
Video amplifiers	Log (4 decades, 35 MHz) and/or wide-band linear
PMT Even-Numbered Dynode Modulation	
Gain compensation	Inverse range squared correction or flat (selectable by front panel control)
PMT 'on' period	1 μs (150 m), 10 μs (1.5 km), 100 μs (15 km), 200 μs (30 km), or variable
Prefull 'on' control	
Step gain (dB down)	0 dB, -10 dB, -20 dB, -30 dB, or -40 dB
Delay from lase	0, 5 μs (750 m), 10 μs (1.5 km), 20 μs (3 km), 30 μs (4.5 km), or variable
Scanning and Firing	
Azimuth and elevation, degree/shot	0.1, 0.2, 0.5, 1.0, 2.0, 5.0, or 10 or by external program
Firing rate, PPM	1, 2, 3, 4, 5, 10, 20, 30, or 60 plus variable (120 PPM available for playback)
Digital processing/recording/display (25-MHz system)	
A/D conversion	Resolution: 8 bits; bit rate: 500 Mb/s (max)
Sample intervals	0.01 μs (1.5 m), 0.02 μs (3 m), 0.05 μs (7.5 m), 0.1 μs (15 m), 0.2 μs (30 m), 0.5 μs (75 m), 1 μs (150 m), and so forth to 10 s (Mixed time base allows increased resolution at range of aerosol of interest.)

Table VI

DIMENSIONS, WEIGHTS, AND POWER CONSUMPTION
OF CRITICAL MARK IX LIDAR TRANSMITTER COMPONENTS

Item Number	Description	Dimensions (inches)	Weight (pounds)	Power
1	Lidar head--shown tilted on its motor-driven pedestal in Figure 23(b)	32 X 26 X 10	180	- - - -
2	Laser control panel (sloping front units)	10 X 10 X 12	10	- - - -
3	Main power unit, for laser and Pockels cell Q switch	33 X 36 X 25	450	230 V, 60 Hz, 1 ϕ. 1600 VA Steady, plus once per pulse load of 6000 to 3000 VA with inductive power factor of 0.3 uncorrected. See text.
4	Refrigerator and water-to-air heat exchangers. Two identical units required. Specification given for one unit.	14 X 18 X 29	100 (including 2.5 gallons of water)	115 V, 60 Hz, 1 ϕ. Refrigerator and circulating pump, 1000 watts for few minutes, dropping to steady 750 W. Heater, adjustable 500-1350 W, cycles off several times per minute.

(a) MARK IX LIDAR VAN

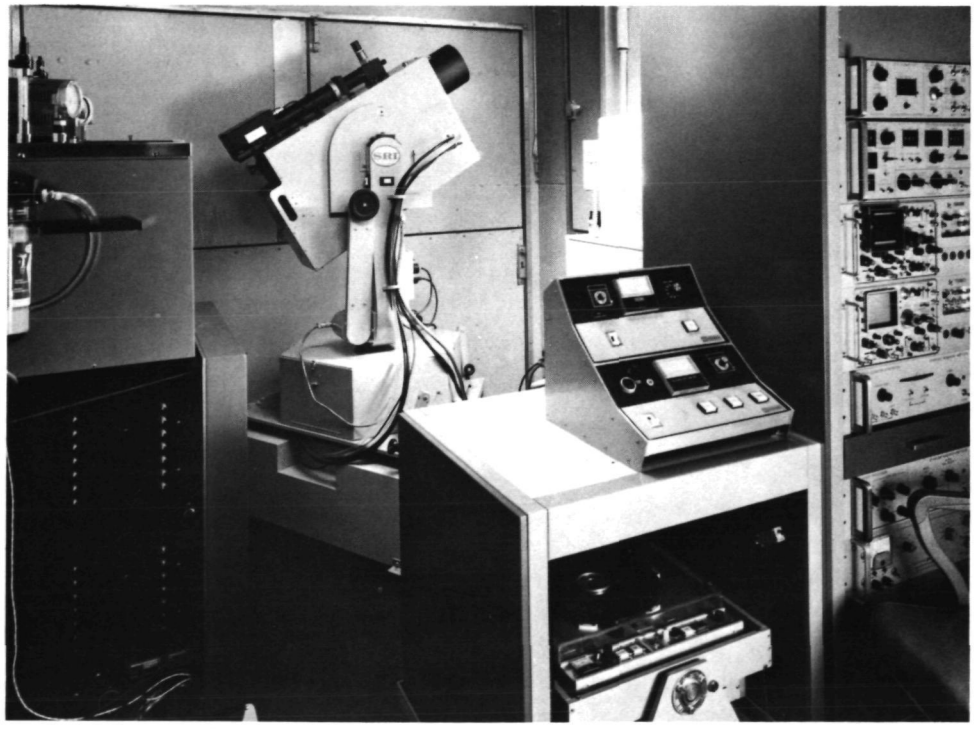

(b) MARK IX LIDAR AND ASSOCIATED ANALOG RECORDING AND DISPLAY ELECTRONICS

SA-1976-1R

FIGURE 23 THE SRI MARK IX LIDAR SYSTEM

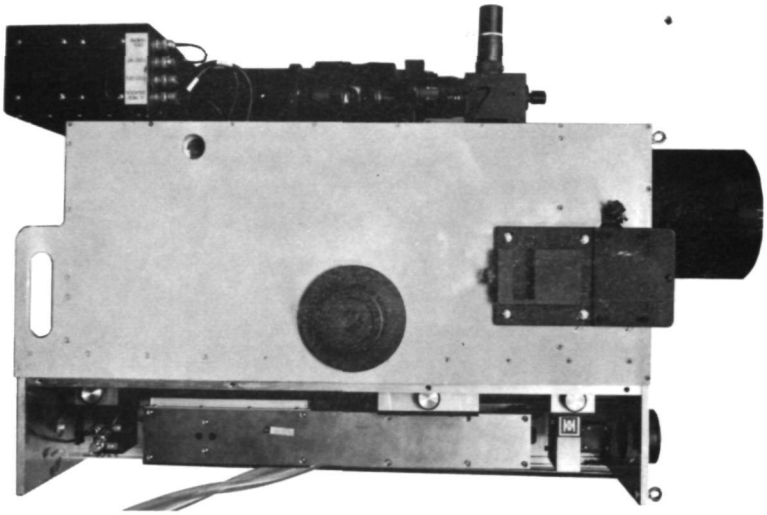

(a) PHOTOGRAPH OF MARK IX LIDAR HEAD

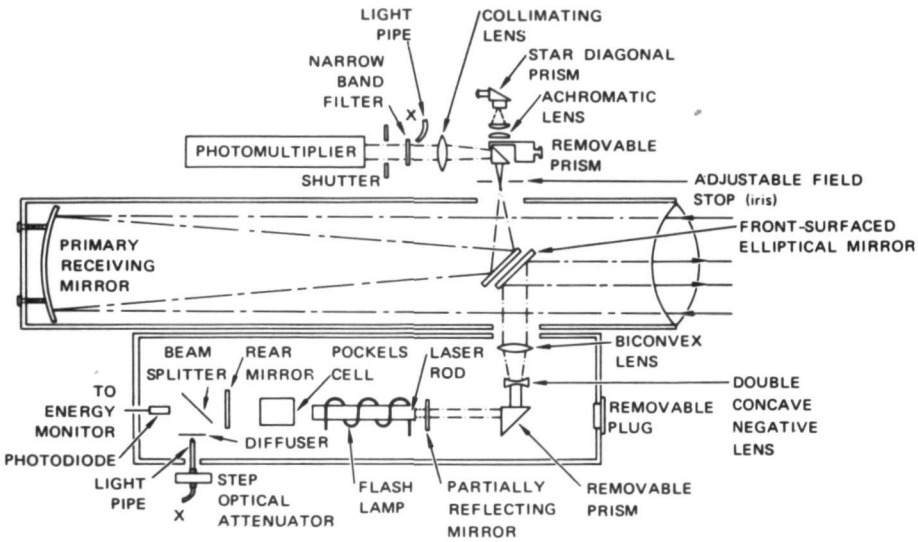

(b) BLOCK DIAGRAM OF MAJOR OPTICAL COMPONENTS

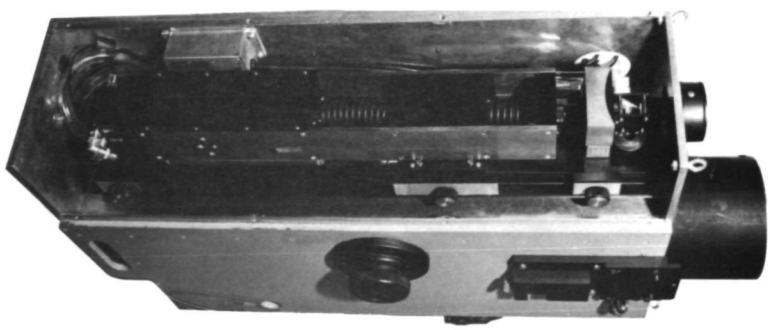

(c) DETAIL OF LASER COMPARTMENT

SA-5557-22

FIGURE 24 HEAD ASSEMBLY FOR THE SRI MARK IX LIDAR

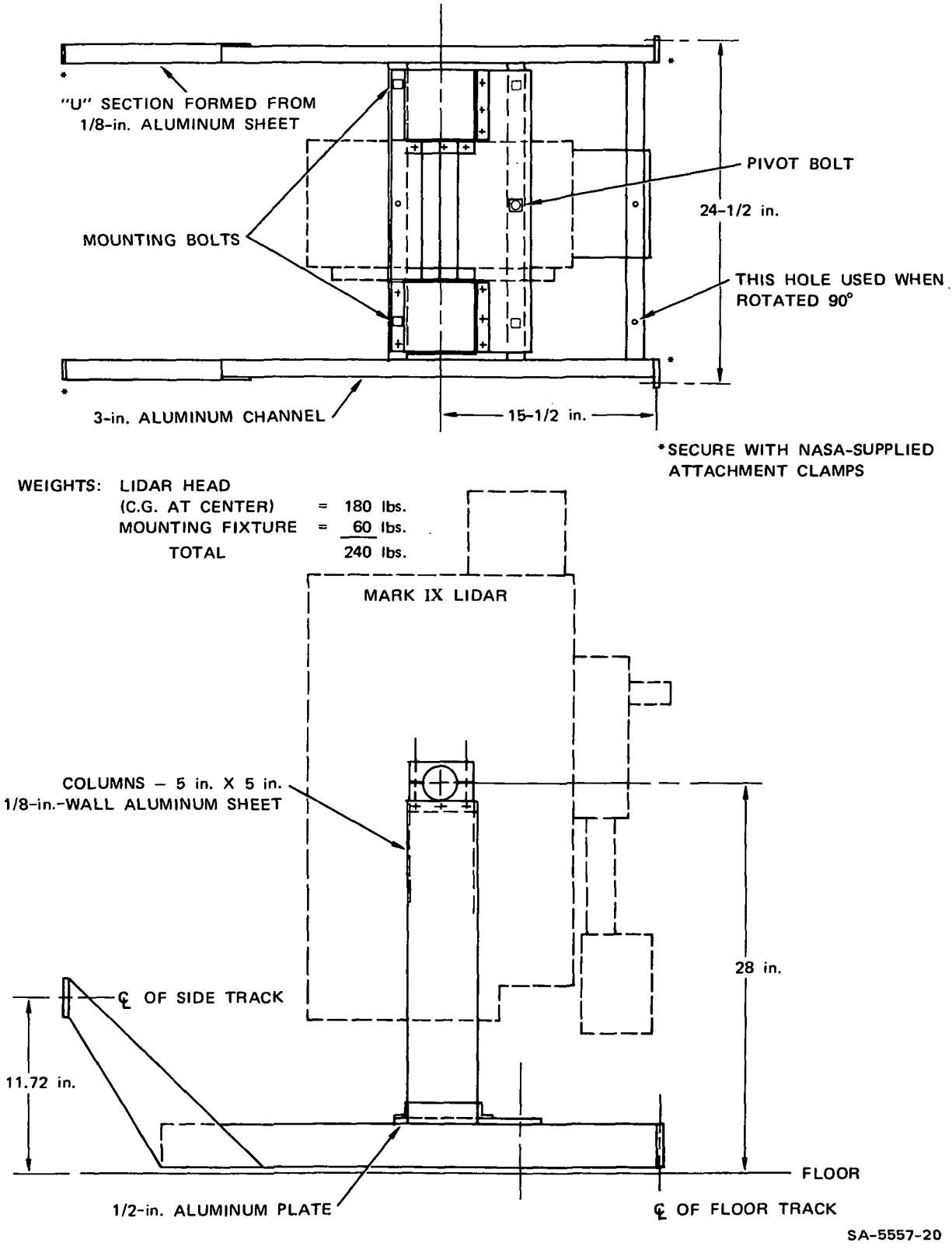

FIGURE 25 MOUNTING FIXTURE FOR MARK IX LIDAR HEAD IN NASA CV990 AIRCRAFT

operation either with the coaxial transmitter/receiver optics of the present lidar system or directly out of the front of the laser (through an upcollimator lens) for use with larger, separately mounted receivers.

Figure 26 is an aircraft floor plan showing a suggested arrangement of the laser transmitter, one or two separate 14" receivers, and all required power supplies, cooling units, and data recording equipment. Separate aluminum channel frames, similar to the one shown for the lidar head are used to secure the main laser power unit (450 pounds), and the water refrigeration system (200 pounds) to the seat tracks. The 14" receivers are intended to be mounted atop standard NASA-supplied "low-boy" equipment racks located under 65° windows.

For a single receiver installation, an operator seated across the aisle from the receiver will be able to reach the convergence adjusting screws of a simple receiver while consulting a storage oscilloscope display in the equipment rack in front of him. This same arrangement could be extended to accomodate a second similar receiver, by locating a seat position and storage oscilloscope adjacent to or across the aisle from the second telescope. For more than two receiving telescopes, remote control of the pointing, as suggested in Section V-F, probably will be required. However, experience may show that stability is good enough so that convergence could be maintained through occasional trimming by a roving operator either carrying a portable storage scope or being coached by telephoned instructions from a second operator at the main panel.

As discussed more completely in Section VII, all of the data processing and recording equipment will fit into one of the standard two-bay NASA/CV 990 equipment racks. Receiver power supplies and miscellaneous drawers can be located in the low-boy racks under the telescopes.

Since these units would be needed even for operation with the present Mark IX coaxial receiver, the minimum floor space required for either of

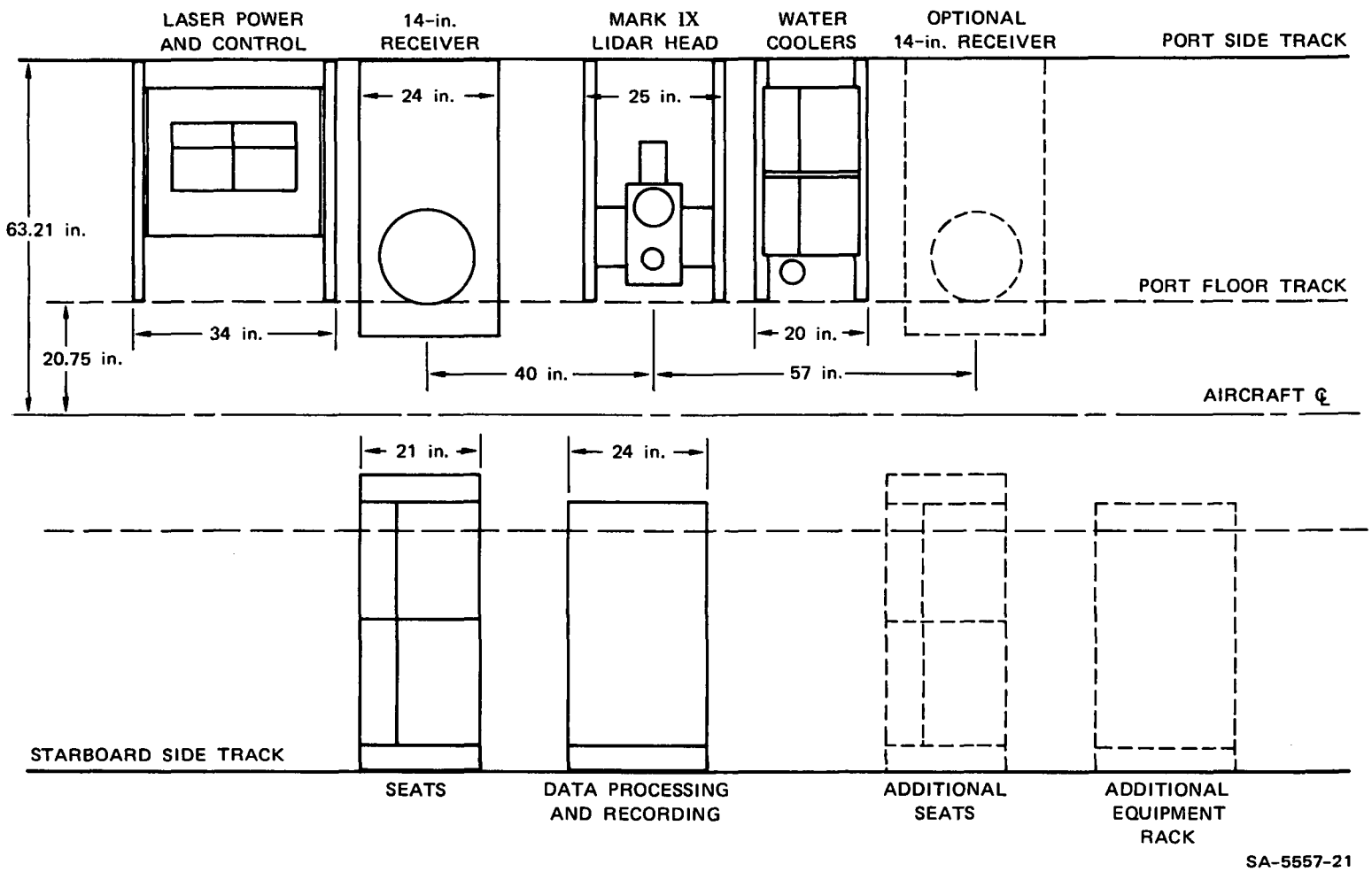

FIGURE 26 LIDAR INSTALLATION IN NASA CV990 AIRCRAFT

Plan view for one-, two-, or three-window options.

those two options (assuming two operators) would be that shown in solid lines in Figure 26. The broken lines indicate the space required for expansion to a two-receiver system or to provide for any additional easily accessible rack space (for CRT photography as an example) that may appear desirable after further experiment planning.

One or two small operator-accessible units (displays, control boxes, and so on) could be added on top of the main equipment rack shown, but if the experiment needs to grow beyond that, a second standard-height equipment rack and seat pair will be required. Each additional receiving telescope station will require only a suitably located low-boy rack. Though not mandatory, seat and control locations would preferably be across the aisle from the equipment, as shown. Any required cross-aisle cabling could be run under the floor, on the floor under a guard tunnel, or across an overhead trough.

Lightweight fiber tubes would extend between the laser transmitter and its overhead window (for eye safety) and between each receiving telescope and its window. Provision should be made to blow heated air through these tubes when required for window defrosting.

2. Electrical Power

The electrical power requirements for the proposed Mark IX 1 pps ruby or Nd: YAG system were given in Table VI. Currently everything operates from 115/230 volt, single phase 60 cycle power.

There is a relatively constant load component of 1500 VA represented by the receiving, data processing, and recording electronics. This load could be serviced by one of the 20 ampere, 115 volt, 60 cycle outlets of the CV 990. The power loads associated with the transmitter and associated water cooling system are both heavier and less constant and will require special consideration.

These loads involve:

- Intermittent, once-per-shot charging of a large 120 joule energy storage capacitor bank. The source voltage is 230 volts, single phase. The input line current begins at 28 amperes rms, drops to 14 amperes rms during approximately 0.8 second, then drops to zero. It has recently been discovered that this current is highly reactive, (power factor of approximately .3, lagging). Thus, the addition of a suitable power factor correction capacitor should reduce the input volt-amperes required for laser firing to about 1/3 of its present value.

- Inductive surges on a 115 volt line resulting from occasional operation of medium sized control relays in the laser power unit.

- Motor loads associated with two small water circulation pumps and two refrigerator motors in the laser cooling system. All of these motors normally run continuously during operation, but produce normal starting transients when first energized.

- A 1350 watt, 115 volt, thermostatically controlled heater which cycles on-and-off intermittently (approximately 1 minute period) to control the water temperature.

When the Mark IX lidar van is operating mobile, all of these surge loads are handled adequately by a 7.5 kva Onan gasoline-driven generator (a second generator supplies air conditioning and all other loads). If the NASA Airborne Science Office at Ames can be persuaded to assign to the laser one of the four 7.5 kva 400-cycle to 60-cycle frequency converters permanently installed in the aircraft, that procedure could provide the simplest solution to the primary power problem. However, the CV 990 Experimenters' Handbook expresses considerable reservation about the surge-handling capability of the CV 990's solid state frequency converters, and states that all requests for such 60 cycle surge loads must be cleared individually with the Ames project manager.

At least two alternatives can be offered for transferring the surge loads to the aircraft main 400 cycle power system where adequate capacity is available.

First, a separate, dedicated, nominal 5 kva converter unit could be procured and installed in the forward cargo compartment in the vicinity of the existing aircraft converters. A suitable unit with a specified ability to handle surge loads is available from Topaz Electronics, San Diego, California (Series FX). This converter weighs 325 pounds, has dimensions of 21" x 19", and costs $4,630.

As a second option, the main capacitor charging circuit in the laser power unit and the cycling 1 kw water heater could be rebuilt to operate from 400 cycle primary power. A smaller, dedicated 400- to 60-cycle converter could then be procured to supply any of the remaining motor or relay loads that could not be handled by the existing aircraft 60 cycle system. A Topaz 2.5 kva converter adequate to handle all of the motor and relay loads when plugged into one of the 2.5 kva 3 phase 400 cycle outlet would weight 240 pounds and cost $3,270. It would be mounted in the low-boy rack that supports the receiving telescope without exceeding weight or stress limitations, or at any other convenient location in the aircraft. Consultation with the supplier of the main power transformer in the laser power supply indicates that the transformer should operate on 400 cycles. This will need to be verified, and the Silicon Controlled Rectifier (SCR) control circuit will need to be suitably modified. A similar conversion was made on an earlier SRI-built 0.3-joule laser and was successfully flown on the first NASA CV 990 for the BOMEX project in 1969. Modification of the cycling 1 kw water heater to operate from one phase of a separate 400-cycle outlet would be straightforward and no problem is anticipated.

This second option is our recommended approach since it would result in less weight, higher efficiency, and fewer components to maintain, and should be obtainable at comparable or lower cost than the first option.

B. High PRF Neodymium System

If the option is exercised to operate with a high PRF Neodymium:YAG laser transmitter (as discussed more completely in Section IX) the transmitter installation would be the one described in that section, the receiver would be any one of the 14-inch options discussed in Section V, and the data processing facility would be as discussed and illustrated in the latter part of Section VII.

IX A NEW LIDAR EMPLOYING A HIGH REPETITION RATE Nd:YAG LASER

A. Transmitter

While an exhaustive survey of all of the many currently available lasers has not been made, the Model 618DR Nd:YAG system manufactured by GTE Sylvania comes well recommended, appears to be representative of the current state of the art, and has been investigated in sufficient detail to determine that it should function well as the transmitter for an airborne stratospheric lidar. It is a compact unit, well engineered for both electrical and optical maintainability, and will operate either from the aircraft 3 phase 400-cycle primary power or from 60-cycle mains for ground-based testing. It employs an oscillator-amplifier combination of two identical and parallel 6.3 x 64 mm (.25 x 2.5 inch) laser rods excited by a single linear flashlamp located between them. (The "DR" in the model number stands for "double rod".) The unit will operate at any rate between single pulse and 300 pulses per second, but the maximum average power (12.5 watts) is obtained at rates between 30 and 50 pps. A photograph and complete specification sheet for the laser is included as Appendix B.

Figure 27 shows a simple mounting arrangement wherein the laser head and a 10x beam expander are contained in a long box that is bolted to the back side of a standard NASA/CV 990 equipment rack so that it fires upward through a 65° window. The problem of cooling requires more attention. The water-to-air heat exchanger that is normally supplied with the laser could be used, perferably after conversion to 400 cycle operation. The 3 kilowatts of dissipated heat would represent a large but apparently tolerable load for the aircraft air conditioning system. One suggestion for relieving this load that came out of discussions with the Ames engineering personnel would be to replace one or two of the side windows with solid aluminum plates and use these as part of a heat

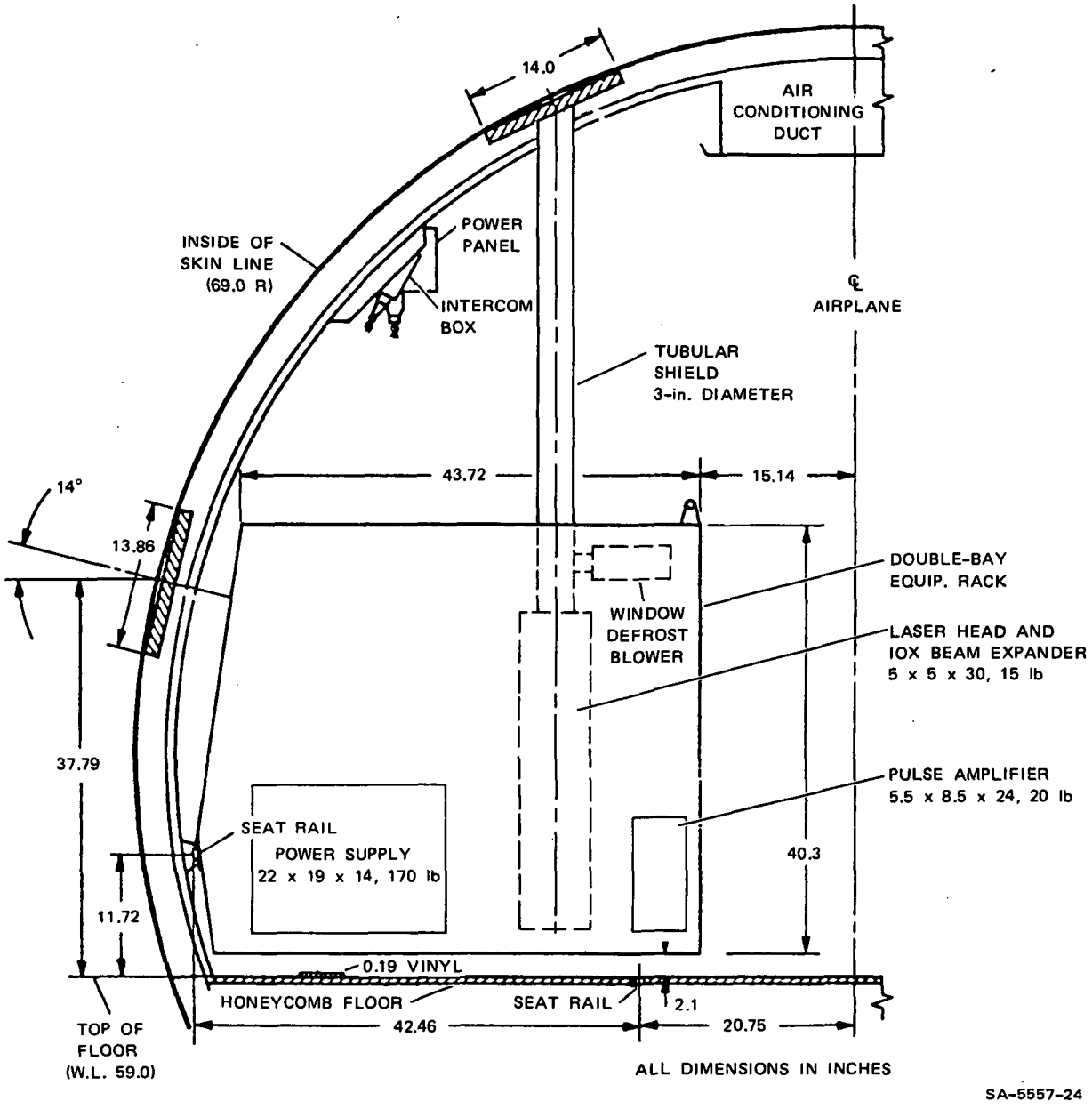

FIGURE 27 HIGH PRF Nd:YAG LASER TRANSMITTER MOUNTED ON STANDARD EQUIPMENT RACK

exchanger to transfer heat from the circulating water to the very cold air outside the aircraft. The water temperature of such a system could be stabilized by a small (approximately 1 kilowatt) refrigerator/heater unit of the type currently used with the Mark IX ruby system. The small unit would have sufficient capacity to support ground testing for short periods or at reduced pulse repetition frequency at times when neither cold outside air nor adequate air conditioning would be available.

B. Receiver, Data Processing, and Recording

The receiving system could be any of the 14-inch options discussed in Section V, and the data processing and recording facility would be as discussed and illustrated in the latter part of Section VII.

X MISCELLANEOUS DESIGN CONSIDERATIONS

A. Mechanical Shutters and Photomultiplier Quirks

Several workers have reported* finding a need to add some form of high speed mechanical shutter to their stratospheric lidars, either at the transmitter to block laser rod fluorescence or at the receiver to prevent strong bursts of light associated with short-range backscattering adversely affecting the PMT internal noise level for periods lasting many tens of microseconds. Sometimes both types of shutter are used. The reported effects were undoubtedly real, since in most cases appreciable work was expended in adding the shutters as retrofits, not as a precautionary measure. On the other hand, in at least four different upper atmosphere probing projects at SRI, involving four different ruby lidar designs, careful performance checks have failed to disclose any significant anomalies due to rod fluorescence. Admittedly, the Mark II lidar was intentionally designed to suppress fluorescence through the placement of a rotating Q switch between the rod and the exit aperture. But for the other three systems, thorough transmitter and receiver light shielding combined with bistatic geometries that made laser-to-receiver transfer via single scattering highly improbable must have provided sufficient attenuation of the fluorescence effect. For the separate-window 14" modular receiver designs proposed herein, unfocused fluorescent radiation from the laser rod would need to traverse a similarly complex, multiple-bounce path to arrive at the detector cathode, and no trouble is anticipated. However

*Refer, for example, to Kent, Clemesha, and Wright (1966), Fiocco and Grams (1966), or Pettifer, Jenkins, Mealey, and Chivery (1976).

should it be encountered, at least two options for cure are open and sufficient time and funds should be allowed so that both options could be implemented, if necessary. First, the Holobeam laser might be rearranged on its optical bench to locate the Pockels cell Q switch between the laser rod and the front etalon. Second, a high speed, rotating shutter could be located between the front etalon and the beam expander and synchronized with the flashlamp/Pockels cell cycle.

Fluorescent lifetimes in Nd:YAG are shorter than in ruby, so trouble at 1.06 microns is considered even more unlikely, though it should certainly be tested for. If fluorescence troubles are encountered with the high repetition rate Sylvania laser, either a synchronized mechanical shutter or a second Pockels cell light valve could be tried.

A similar contingency factor must be included to test for transient-induced noise effects in the Varian photomultipliers. These tubes are new, and no specification exists to cover the specialized condition of brief, intense light exposure closely followed by attempts to make accurate measurements of extremely low light levels-in the photon counting regime. Historically, photomultipliers have displayed both family characteristics and individual traits in their transient and noise performance.

Pettifer (1975), using a 56TUVP tube, found spurious noise counts amounting to as much as 5% of the inducing signal level in the range bin following a cathode irradiance pulse of only 10^{-13} watt/cm^2, an effect that can hardly be ignored. However, Young (1976) making similar tests on an EMI 9558B photomultiplier found the effect to be some two orders of magnitude less severe and thus ordinarily negligable.

Experience at SRI with ITT, Amperex, and RCA photomultipliers has been that the proposed technique of keeping the tube gain low (by unbalancing the dynode potentials) except for the brief period where high gain is required has been effective in reducing some types of afterpulsing.

This is particularly true of the spurious responses occurring after the extremely high light pulses that may be encountered in lower troposphere lidars, on the order of $> 10^{-3}$ watts/cm^2. There is, however, no assurance that these two noise-generating mechanisms are related or that either is representative of what will be encountered with the high quantum efficiency Varian photomultiplier tubes. Careful performance tests on controlled lidar-like light pulses will need to be part of the detailed design and construction phase.

If a fast receiving shutter is found necessary it should be located close to the photomultiplier so that only one would be required, even for a multiple telescope system. The implementation of such a shutter would not be a trivial matter. At its most accessible region, the light for either the close-coupled design of Figure 12 or at the exit end of a group of light fibers in a multiple receiver design would be several milimeters in diameter. To uncover such a beam within a time period of, say, 30 microseconds would require a shutter speed of approximately 100 meters/second requiring, at the minimum, an 8 cm diameter shutter running at 24,000 rpm (Pettifer used an 11.4 cm shutter at 24,000 rpm). For aircraft use, the centrifugal forces associated with such high shutter speeds will present an additional problem to be watched.

The proposed receiver design includes two other shutters. A solenoid-operated slide that is ahead of the focal plane and is spring-closed during stand-by periods prevents heating of internal components should aircraft maneuvers point the telescope toward the sun. It would also be desirable to have this shutter close if average PMT anode current becomes excessive. A simple shutter or dark slide on the PMT housing is essential to keep the tube dark during times when the housing is removed from the lidar.

B. Window Damage Thresholds

In addition to the transmission tests made on CV 990 optical windows (Section V-G), SRI has previously tested for mechanical damage by

repeatedly firing 0.5 joule pulses in a 2" diameter beam through window samples of all glasses supplied. The average energy density was .025 J/cm^2. The windows successfully survived both the Ames vacuum tank test and many succeeding aircraft flights.

Data on mechanical damage thresholds for various optical glasses have since been published by Alexander (1975). This source indicates that laser energy densities in the range of 50-150 J/cm^2 normally are required to effect damage, though the presence of surface dust or internal flaws can reduce the threshold. The maximum beam energy density proposed in this report is 0.09 J/cm^2 (for the unmodified Mark IX ruby system). All other systems involve both larger beams and lower pulse energies. However the average power level for the high repetition rate Nd:YAG system would be sufficiently high that it would be prudent to run a demonstration test through a dirty window as a safety measure. (Engine oil deposits on the windows have caused problems in previous flights of the CV990.)

C. Possible Use of Silicon Diode Photodetector

Improvements continue to be made in the development of the silicon avalanche diode (SAD) as a solid state counterpart of the vacuum-filled multiplier phototube.

While the ruggedness, small size, the much more modest power supply requirements, and the relative freedom from thermal emission effects are all attractive attributes of these devices, by far the most enticing feature for atmospheric lidar applications is the high quantum efficiency that can be obtained in the near infrared--30% to 60% at 1.06 micrometers by comparison with 2% for the Varian InGaAsP photocathode or .05% for the older S1 photomultiplier tubes.

Unfortunately, however, the gain and gain stability performance of available avalanche diodes, when combined with the thermally-induced input noise of a succeeding video amplifier, are such that the realizable overall signal-to-noise performance is still significantly less than for thoroughbred photomultipliers for low background applications.

For example, an LE-104 avalanche diode/amplifier combination device offered by General Electric has a quoted Noise Equivalent Power (NEP) of 2.5×10^{-10} watts at a bandwidth of 1 MHz and a wavelength of 1.06 micrometers. To examine this number in the context of an airborne stratospheric lidar, we recall (with the aid of Figure 3) that for an aircraft flying at 10 km the Rayleigh-backscattered return from a 1 joule Neodymium transmitter into a 14" aperture receiver via an air mass at an altitude of 22 km is 3.8×10^{-11} watts and that the incoming background light will be negligibly small by comparison, even in the daytime. It is, moreover, not this absolute signal level but the fluctuation component or rms uncertainty in measuring the signal amplitude that must be compared with NEP. If a VPM 164A photomultiplier is used to measure the received radiation, and an integration period of 1 microsecond is used (to be compatible with the above-specified 1 MHz bandwidth of the solid state SAD device), the total number of pulses counted per 150 meter range increment will be 10 and the uncertainty will be 3.16 counts, which transforms back to an equivalent uncertainty or quantum noise component of 1.2×10^{-11} watts for the actual 1.06 micron radiation input.

Thus, for this example, the silicon avalanche diode device is still noisier over an order of magnitude than the state-of-the-art photomultiplier. There are things that can yet be done to improve the avalanche diode performance; the quantum efficiency can be improved by heating, the amplifier noise can be lowered by cryogenic cooling, and the gain and gain stability (excess noise factor) may be further improved through device design, but no proven unit known to the author is yet fully competitive with the PMT. One of the leading developers of SAD technology, R.J. McIntyre (1972), has pointed out that it is possible to operate some avalanche photodiodes in a photon counting mode by increasing the gain to the point of regenerative breakdown, in a "Geiger-tube", mode, thereby realizing a responsivity of a phenominal 50 volts/photon without further amplification, and yielding

detection probabilities comparable to the best available photomultipliers. Even if this were a possibility for the very low count rates associated with very high altitude lidar returns, the requirement for a finite recovery time between photon events would leave a sizeable operating gap between radiation levels amenable to photon counting and those amenable to analog recording with silicon avalanche diode devices, that is, for situations when the background radiation level is much greater than it is for the cases of interest here.

D. Reference Optical Attenuator

Standard on the Mark IX and nearly all recent SRI lidars is a fiber optic light path that takes a very small sample from the transmitted light pulse, passes it through an adjustable optical attenuator, then on to the PMT, by-passing all other optical components. Once the passive attenuator has been "calibrated", by comparison to the lidar Rayleigh return from a reference altitude under optimum operating conditions, it provides a round-trip path and system attenuation bench mark that can later be used as a rapid check of overall system performance or as a means of approaching an absolute calibration of the lidar. It is recommended that some similar optical reference path be incorporated into the proposed modular receiver design. The reference path fiber could conveniently enter the PMT housing bundled along with the signal-carying fibers.

XI COST ESTIMATES

Bugetary estimates of costs associated with the several options discussed in this study are given below.

Option 1 Fly Mark IX Lidar

Install existing SRI Mark IX Lidar system in the NASA CV 990 aircraft. Rent the required major components not now a part of the Mark IX lidar, (for example, 9-track tape recorder, 400 Hz to 60 HZ power converter.) Operate and acquire data (analog mode only) during three test flights.

.....$40,000

Option 2 14-Inch Receiver Module (Master)

Construct and test a 14-inch lidar receiver module, including a four-quadrant convergence monitoring system to facilitate operating with a separately-located laser transmitter. Procure a high performance photomultiplier tube such as the Varian VPM 164M or VPM 192M and provide a detailed evaluation of the applicability of that detector for upper atmosphere lidar, in both pulse counting and analog recording modes. The design may use either direct or fiber optic coupling between the telescope and the main signal detector, but should be expandable to permit slaving additional telescopes to the detector via fiber optic coupling.

.....$43,000 with VPM 164M
.....$39,000 with VPM 192M

Option 3 Slave 14-Inch Receivers

Supply additional 14-inch receiver modules, following the design of Option 2 and intended to be slaved to it via fiber optic coupling for both the main signal and convergence monitoring. No additional detectors will be required.

.....$11,500 each

Option 4 PMT Signal Processor

Design, construct, check out, and document a photomultiplier pulse integrator assembly following the general approach outlined in Section VII of this report.

.....$26,000

Option 5 Convert Mark IX Lidar to 1.06 μ

Convert the SRI Mark IX lidar transmitter for operation at 1.06 micrometer wavelength, using a Nd:YAG rod. Nominal output shall be 1 joule at 1 pulse/second. Reusable components will become government property.

.....$8,600

Option 6 New High PRF Nd:YAG Lidar

Provide a complete airborne lidar facility following the general design given in Section IX of this report. The lidar to consist of:

A high PRF (10-100 pps) Q switched Nd:YAG laser transmitter capable of operation for extended periods at an average output power of approximately 10 watts.

One 14-inch modular receiver, similar to that of Option 2, but employing a cooled VPM 164A photomultiplier.

A digital data acquisition system, employing principally Digital Equipment Company PDP 11/03 hardware and following the design generally outlined in Section IX of this report, combined with pulse integration circuitry similar to that of Option 4.

.....$245,000

Option 7 Augmented Mark IX System

Provide a high performance, 1 joule, 1 pps ruby system with a separate 14-inch receiver by combining Options 1, 2, and 4 plus a storage oscilloscope.

.....$113,000

XII CONCLUSIONS AND RECOMMENDATIONS

While final decisions about the level of equipment performance to be specified for the proposed airborne stratospheric lidar system should await review of the data presented herein by the SAM-II Nimbus Experiment Team (NET), this study concludes that the existing Mark IX lidar system would be of limited utility even if its data processing and recording system were modified to operate in both analog and pulse counting modes. A significant increase in system performance could be obtained by providing a new receiver that would more effectively utilize the limited aperture area of available aircraft windows and also would utilize the improved quantum efficiency and noise characteristics of modern high performance photomultipliers. This change would result in an increase in the number of detected photoelectrons per transmitter pulse by approximately 28 times. Still better receiver performance could be achieved by two or more telescopes operated essentially in parallel by means discussed herein.

The lidar receiver designs suggested by this study for achieving these higher levels of system performance entail three major risk areas and it is recommended that these risk areas be investigated more thoroughly as the next step in the development.

First, the actual operating performance of one or more samples of the recommended Varian photomultiplier tubes should be examined with pulsed light signals simulating the wide dynamic range anticipated from the lidar. These tests will determine not only the inherent amplitude linearity of the detector, but also whether a high speed rotating shutter will be required in the receiver to suppress the shock effect of strong near-field lidar returns.

Second, it should be determined whether the analog pulse integration and PMT gain switching schemes proposed herein can be made to operate reliably over the required large dynamic range and with the selected

photomultiplier. The results should be compared with the more conventional approach of digital pulse counting at the longer ranges combined with a separate analog recording system for shorter ranges before the final data recording system is specified.

Third, if it is determined that receiving apertures larger than can be achieved through a single aircraft window are desirable, then the extent to which the proposed multiple-telescope scheme could be expanded should be investigated by making some simple in-flight measurements of aircraft flexing using a low-power cw laser and/or a theodelite.

Investigation into these three risk areas would be equally applicable to a lidar system implemented with either the present Mark IX laser transmitter or with a new transmitter of higher average power and pulse rate. This choice will be dictated primarily by factors of budget and time scheduling.

REFERENCES

C.W. Allen, Astrophysical Quantities (Univ. of London, Athlone Press, 1955).

R.J. Allen and W.E. Evans, "Laser Radar (LIDAR) for Mapping Aerosol Structure," Rev. Sci. Instr., Vol. 43, pp. 1422-1432 (1972).

S.Q. Duntley, "Aerial Measurements of Atmospheric Clarity and Sky Luminance Near Alamogordo, New Mexico," Final Report AD 640 003, U.S. Dept. of Commerce, National Bureau of Standards, Institute for Applied Technology (1958).

G. Fiocco and G. Grams, "Observations of the Upper Atmosphere by Optical Radar in Alaska and Sweden During the Summer 1964," Tellus, Vol. 18, pp. 34-38 (1966).

G.S. Kent et al., "High Altitude Atmospheric Scattering of Light from a Laser Beam," J. Atmos. Terrest. Phys., Vol. 29, pp. 169-181 (1967).

R.J. McIntyre, "The Distribution of Gains in Uniformly Multiplying Avalanche Photodiodes: Theory, IEEE Trans. Electron Devices, Vol. Ed-19, No. 6, pp. 703-713 (1972).

NASA/Ames Research Center: Airborne Laboratory Experimenters' Handbook, NASA CV-990 (April 1975). (Available from Airborne Science Office, Moffett Field, California.)

R.E. Pettifer, "Signal Induced Noise in Lidar Experiments," J. Atmos. Terrest. Phys., Vol. 37, pp. 669-673 (1975).

R.E. Pettifer et al., "A Large Coaxial Lidar for Elastic and Ineleastic Scattering Studies of the Stratosphere," to appear in Opt. and Quantum Electron. (1976).

R.G. Pinnick et al., "Stratospheric Aerosol Measurements 111: Optical Model Calculations," J. Atmos. Sci., 33 pp. 304-314 (1976).

G. Quasius and F. McCanless, Star Trackers and Systems Design, (Spartan Books, Washington 1966).

Russell, P. B.; Viezee, W.; Hake, R. D., Jr.; and Collis, R. T. H.: Lidar Observations of the Nonvolcanic Stratospheric Aerosol: California, October 1972-March 1974. Quart. J. Roy. Meteorol. Soc., Vol. 102, pp. 619-639, 1976a.

Russell, P. B.; Hake, R. D., Jr.; and Viezee, W.: Lidar Measurements of the Post-Fuego Stratospheric Aerosol. Final Report, Project 4019, Stanford Research Institute (Menlo Park, California), 1976b.

U.S. Air Force: The Handbook of Geophysics. Macmillan, Co., rev. 1960.

U.S. Air Force: Handbook of Geophysics for Air Force Designers, USAF Cambridge Research Center, 1957.

Young, S. A.: Signal Induced Noise in Photomultipliers Used in Lidar Receivers, J. Atmos. Terrest. Phys., Vol. 38, pp. 667-670, 1975.

Appendix A

CALCULATIONS FOR TEST CASES DISCUSSED AND SUMMARIZED IN SECTION III-C

Appendix A

CALCULATIONS FOR TEST CASES DISCUSSED AND SUMMARIZED IN SECTION III-C

Case 1

1 joule Ruby

14" Receiver

H = 20 km, R = 10 km

Cross Polarized Receiver

ΔR = 0.5 km (3.33 μsec), T_{pmt} = +20°C

$$S_P/N = \frac{N_P}{\sqrt{N_P + N_R + N_B + N_I}} = \frac{288 \times 3.33}{\sqrt{3.33\ (288 + 566 + 0.6 + 0.08)}}$$

$$= \frac{959}{\sqrt{959 + 1887 + 2 + 0.27}} = \frac{959}{53.4} = 17.97 \quad .$$

For $S_P/N = 100$, we should integrate $(100/17.97)^2$ = 31 shots. Thus, at a PRF of 1 pps, 31 seconds would be required to measure β_P to a precision of 1%.

Alternatively,

$$S_T/N = \frac{N_R + N_P}{\sqrt{N_P + N_R + N_B + N_I}} = \frac{3.33\ (288 + 566)}{\sqrt{3.33\ (288 + 566 + 0.6 + 0.8)}}$$

$$= \frac{2844}{\sqrt{2846}} = 53.3 \quad .$$

For $S_T/N = 100$, we should integrate $(100/53.3)^2$ = 3.5 shots. Thus, at PRF of 1 pps, 3.5 seconds would be required to measure β_P to a precision of the local $\beta_T = \beta_P + \beta_R$.

Variations:

If we use an unpolarized receiver, sky background N_B will go up by a factor of 10. All other factors are unchanged.

$$S_p/N = \frac{959}{53.6} = 17.89 \quad .$$

For $S_p/N = 100$, need to integrate 31.2 shots.

Conclusions:

(1) Room temperature OK for PMT

(2) Negligible improvement by using polarized receiver.

Case 2

1 joule Nd:YAG

14" Receiver

H = 20 km R = 10 km

Cross polarized receiver

ΔR = 0.5 km (3.33 μsec), T_{pmt} = -20°C

$$S_P/N = \frac{N_P}{\sqrt{N_P + N_R + N_B + N_I}} = \frac{3.33\ (38)}{\sqrt{3.33\ (38 + 21 + 0.008 + 0.001)}}$$

$$= \frac{126}{\sqrt{196.7}} = 8.98 \quad .$$

For $S_P/N = 100$, we should integrate $(100/8.98)^2$ = 123.9 shots. Thus, at a PRF of 1 pps, 2.1 minutes would be required to measure β_P to a precision of 1%.

Alternatively,

$$S_T/N = \frac{N_R + N_P}{\sqrt{N_P + N_R + N_B + N_I}} = \frac{3.33\ (38 + 21)}{\sqrt{3.33\ (38 + 21 + 0.008 + 0.001)}}$$

$$= \frac{196}{\sqrt{196.7}} = 14.0 \quad .$$

For $S_T/N = 100$, we should integrate $(100/14)^2$ = 51 shots. Thus, at a PRF of 1 pps, 51 seconds would be required to measure β_P to a precision of 1% of the local $\beta_T = \beta_P + \beta_R$.

Variations:

If we use an unpolarized receiver, sky background will increase by factor of 10. All other figures stand.

$$S_P/N = \frac{126}{\sqrt{196.9}} = 8.98 \text{ (same as above).}$$

Conclusions:

(1) Negligible improvement by using polarized receiver.

(2) Negligible improvement by using cooled PMT, but the IR PMT must be cooled to avoid deterioration.

Case 3

0.3 joule Nd:YAG (High PRF)

14" receiver

H = 20 km R = 10 km

Cross polarized receiver

ΔR = o.5 km (3.333 μsec), T_{pmt} = -20°C

$$S_P/N = \frac{N_P}{\sqrt{N_P + N_R + N_B + N_I}} = \frac{3.33\ (11.4)}{\sqrt{3.33\ (11.4 + 6.3 + 0.008 + 0.0001)}}$$

$$= \frac{38.0}{\sqrt{38 + 21 + 0.027 + 0.0003}} = \frac{38}{\sqrt{59.027}} = 4.95 \quad .$$

For $S_P/N = 100$, need to integrate $(100/4.95)^2$ = <u>408.8 shots</u>. Thus, at a PRF of 30 pps, 13.6 seconds would be required to measure β_P to a precision of 1%.

Alternatively,

$$S_T/N = \frac{3.33\ (11.4 + 6.3)}{\sqrt{59.07}} = 7.67 \quad .$$

For $S_T/N = 100$, we should integrate $(100/7.7)^2$ = <u>170 shots</u>. Thus, at a PRF of 30 pps, 5.7 seconds would be required to measure β_P to a precision of 1% of the local $\beta_T = \beta_P + \beta_R$.

<u>Variations</u>:

If we use an unpolarized receiver, sky background will go up by a factor of 10. All other figures stand.

$$S_P/N = \frac{38}{\sqrt{59.27}} = 4.94 \quad .$$

For $S_P/N = 100$, need $(100/4.94)^2$ = <u>410.5 shots</u>.

<u>Conclusions</u>:

(1) Extremely slight improvement in using polarized receiver.

(2) PMT cooling not required for S/N, but necessary to avoid deterioration.

Case 4

Unmodified Mark IX Ruby Lidar

H = 20 km R = 10 km

ΔR = 0.5 km (3.33 μsec), T_{pmt} = +20°C

Cross polarized receiver

$$S_P/N = \frac{N_P}{\sqrt{N_P + N_R + N_B + N_I}} = \frac{3.33\ (8.36)}{\sqrt{3.33\ (8.36 + 16.4 + 0.19 + 0.05)}}$$

$$= \frac{27.87}{\sqrt{27.87 + 54.67 + 0.633 + 0.167}} = \frac{27.87}{\sqrt{83.34}} = 3.053 \quad .$$

To get $S_P/N = 100$, need to integrate for $(100/3.053)^2$ = 1073 shots. Thus, at a PRF of 1 pps, 17.9 minutes would be required to measure β_P to a precision of 1%.

Alternatively,

$$S_T/N = 9.03 \quad .$$

For $S_T/N = 100$, we should integrate $(100/9.03)^2$ = 122.6 shots. Thus, at a PRF of 1 pps, 2.0 minutes would be required to measure β_P to a precision of 1% of the local $\beta_T = \beta_P + \beta_R$.

Conclusions:

(1) While sky and internal noise are not completely negligible, by far the biggest uncertainty is due to the low quantum count in the signal.

(2) The integration times may be too long to be useful for a SAM-II operation, but should suffice for a baseline test run.

Case 5

How long would we need to integrate to get a 1% reading on the Rayleigh return from 80 km?

1 joule Ruby

14" receiver

H = 80 km R = 70 km

Cross polarized receiver

ΔR = 0.5 km (3.33 μsec), T_{pmt} = +20°C

$$S_P/N = \frac{N_R}{\sqrt{N_R + N_B + N_I}} = \frac{3.33\ (0.03)}{\sqrt{3.33\ (0.03 + 0.6 + 0.08)}} = \frac{0.0999}{\sqrt{2.366}} = 0.065 \quad .$$

For $S_R/N = 100$, need to integrate for $(100/0.065)^2 = \underline{2.4 \times 10^6 \text{ shots}}$ (657 hours @ 1 pps).

Conclusions:

(1) Integration time completely excessive.

(2) Daytime light biggest contributor to noise. Internal noise next, but this could be reduced by cooling.

Case 6

How long would we need to integrate to get a 1% reading on particulates at H = 40 km?

1 joule Ruby

14" receiver

H = 40 km R = 30 km

Cross polarized receiver

ΔR = 0.5 km (3.33 μsec), T_{pmt} = -20°C

$$S_P/N = \frac{N_P}{\sqrt{N_P + N_R + N_B + N_I}} = \frac{(3.33)\ 0.04}{\sqrt{3.33\ (0.04 + 3 + 0.6 + 0.0001)}}$$

$$= \frac{.13333}{\sqrt{0.1333 + 9.999 + 1.999 + 0.0003}} = \frac{.1333}{\sqrt{12.134}} = 0.038 \quad .$$

For $S_P/N = 100$, need to integrate for $(100/0.038)^2 = \underline{6.8 \times 10^6}$ shots. Thus, at a PRF of 1 pps, 1895 hours would be required to measure β_P to a precision of 1%.

Alternatively,

$$S_T/N = \frac{N_P + N_R}{\sqrt{N_P + N_R + N_B + N_I}} = \frac{3.33\ (0.04 + 3)}{\sqrt{3.33\ (0.04 + 3 + 0.06 + 0.0001)}} = 2.90 \quad .$$

For $S_T/N = 100$, we should integrate $(100/2.9)^2 = \underline{1.2 \times 10^3\ \text{shots}}$. Thus, at a PRF of 1 pps, 19.8 minutes would be required to measure β_P to a precision of 1% of the local β_T ($\approx \beta_R$).

Case 7

1 joule Nd:YAG

14" receiver

H = 40 km R = 30 km

Cross polarized receiver

ΔR = 0.5 km (3.33 μsec), T_{pmt} = -20°C

$$S_P/N = \frac{N_P}{\sqrt{N_P + N_R + N_B + N_I}} = \frac{3.33\ (0.005)}{\sqrt{3.33\ (0.005 + 0.1 + 0.008 + 0.0001)}}$$

$$= \frac{0.0167}{\sqrt{(0.0167 + 0.3333 + 0.0266 + 0.0003)}} = \frac{0.0167}{\sqrt{0.3767}} = 0.0272 \quad .$$

To get $S_P/N = 100$, need $(100/0.0272)^2 = \underline{13.5 \times 10^6 \text{ shots}}$ (3750 hours @ 1 pps).

Alternatively,

$$S_T/N = \frac{3.33\ (0.1 + 0.005)}{\sqrt{3.33\ (0.005 + 0.1 + 0.008 + 0.0001)}} = 0.545 \quad .$$

To get $S_T/N = 100$, need $(100/0.545)^2 = \underline{3.36 \times 10^4 \text{ shots}}$. Thus, at a PRF of 1 pps, 9.34 hours would be required to measure β_P to a precision of 1% of the local β_T ($\approx \beta_R$).

Variations:

What can we do with ΔR = 5 km and 10% accuracy?

$$S_P/N = \frac{0.167}{\sqrt{3.767}} = 0.086$$

$$\left(\frac{10}{0.086}\right)^2 = \underline{13{,}507 \text{ shots}} \text{ (3.75 hours @ 1 pps).}$$

Alternatively,

$$S_T/N = \frac{3.50}{\sqrt{3.767}} = 1.80$$

$$\left(\frac{10}{1.80}\right)^2 = \underline{31 \text{ shots}} \text{ (31 seconds @ 1 pps).}$$

Thus, at a PRF of 1 pps, 31 seconds would be required to measure β_P to a precision of 10% of the local β_T ($\approx \beta_R$).

Case 8

How long must one integrate to get 10% reading on particulates with Ruby system at H = 40 km?

1 joule Ruby

14" receiver

H = 40 km R = 30 km

Cross polarized receiver

ΔR = 5 km (33.33 μsec), T_{pmt} = -20°C

$$S_P/N = \frac{N_P}{\sqrt{N_P + N_R + N_B + N_I}} = \frac{1.333}{\sqrt{1.333 + 99.99 + 19.999 + 0.003}}$$

$$= \frac{1.333}{\sqrt{121.34}} = 0.121 \quad .$$

For $S_P/N = 10$, need to integrate $(10/0.121)^2$ = 6825 shots (1.9 hours @ 1 pps).

Alternatively,

$$S_T/N = \frac{101.33}{\sqrt{121.34}} = 9.16 \quad .$$

For $S_T/N = 10$ need to integrate $(10/9.16)^2$ = 1.2 shots (1.2 seconds @ 1 pps).

Case 9

.1 joule Nd:YAG @ 30 pps

Seven 14" receivers

H = 40 km R = 30 km

Cross polarized receiver

ΔR = 5 km (33.33 μsec), T_{pmt} = -20°C

$$S_P/N = \frac{N_P}{\sqrt{N_P + N_R + N_B + N_I}} = \frac{33.3\ (0.005)\ (0.3)\ (7)}{\sqrt{33.3\ (0.3)\ (7)\ (0.005 + 0.1 + 0.008 + 0.0001)}}$$

$$= \frac{0.350}{\sqrt{0.350 + 7.0 + 0.56 + 0.007}} = \frac{0.350}{\sqrt{7.917}} = 0.124 \quad .$$

To get $S_P/N = 10$, we need:

$$\left(\frac{10}{0.124}\right)^2 = \underline{6463\ \text{shots}}, \text{ or 3.6 minutes @ 30 pps.}$$

Alternatively,

$$S_T/N = 2.60 \quad .$$

To get $S_T/N = 10$, we need $(10/2.6)^2 = \underline{15\ \text{shots}}$, or 0.5 seconds at 30 pps.

Appendix A

Table A-1

SUMMARY SHEET FOR TEST CASES[a]

	Case Number												
	1	1A	4	5	6	8	2	2A	3	3A	7	7A	9
Transmitter													
λ, μm	.694 →						1.060 →						
Pulse energy, J	1 →								.3 →		1 →		.3
PRF, s^{-1}	1 →								30 →		1 →		30
Receiver													
Nominal diameter, in.	14 →		6 →	14 →									7 × 14
q.e.	0.15 →		.02 →	.15 →			.02 →						
ΔR, km	0.5 →					5 →	.5 →					5 →	
Day/night	Day →												
Altitude, km	20 →		80 →	40 →			20 →				40 →		
Cross-polarized?	Yes	NO	Yes →					No	Yes	No	Yes →		
Electron counts/range bin													
N_P	959 →		28 →		.13	13	126.7 →		38 →		.02 →		.35
N_R	1887 →		55	.1	10	100	70 →		21 →		.33 →		7
N_B	2 →		.63	2	2	20	.027 →		.27 →		.03 →		.56
N_I	0.27 →		.17	.3	.0003	.003	.0003 →		.0003 →		.003 →		.007
Single shot S_P/N	17.97	17.89	3.05	.065	.04	.121	8.98	8.98	4.95	4.94	.027	.086	.124
Single shot S_T/N	53.3		9.03	.065	2.90	9.16	14.0		7.67		0.55		2.6
% Precision	1 →					10	1 →					10 →	
Time to achieve specified precision in β_P	31s	31.2s	18 min	657h	1895h	1.9h	124s	124s	13.6s	13.6s	3750h	3.75h	3.6 min
Time to achieve specified precision in R[b]	3.5s	3.5s	2.0min	657h	19.8min	1.2s	51s		5.7s	5.7s	9.34h		0.5s

[a]Arrows indicate duplication of entries.

[b]The time required to achieve a precision of x% in scattering ratio R is the same as the time required to measure β_P to a precision of x% of β_T ($=\beta_P + \beta_R$)

Appendix B

PHOTOGRAPH AND SPECIFICATION FOR HIGH PRF Nd:YAG LASER

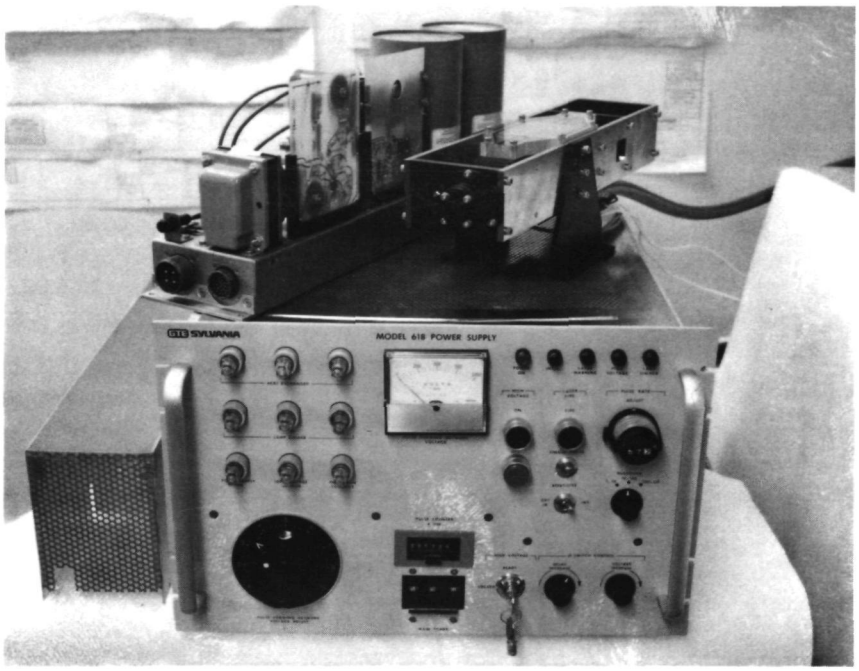

SA-5557-25

FIGURE B-1 SYLVANIA MODEL 618DR PULSED Nd:yag LASER

Table B-1
DESIGN SPECIFICATIONS
SYLVANIA MODEL 618DR LASER

TYPE:	Nd:YAG, pulsed, Oscillator-Amplifier, Q-Switched
WAVELENGTH:	1.064 micrometers
P.R.F.:	Continuously variable, single shot to 100Hz
OUTPUT PULSED ENERGY:	> 300 mj/pulse to 50Hz; 150 mj/pulse at 100Hz Pulse to pulse stability, ± 5%
PULSE DURATION:	< 25ns (FWHM)
BEAM DIAMETER:	6mm
BEAM DIVERGENCE:	< 4 miliradians
INPUT POWER:	50/60Hz or 400Hz; 208V, 3 phase 3200 watts, including water/air heat exchanger
DIMENSIONS AND WEIGHTS:	Resonator, 17.5 x 5 x inches, 15 pounds Head Amplifier, 24 x 5.5 x 8.5 inches, 20 pounds Power Supply, 10.5 x 19 x 19.5 inches, 170 pounds Water/air heat exchanger, 22 x 12 x 19 inches, 65-90 pounds